

1 **KDM6B promotes activation of the oncogenic CDK4/6-pRB-E2F pathway by maintaining**  
2 **enhancer activity in MYCN-amplified neuroblastoma**

3

4

5 Alexandra D'Oto<sup>1\*</sup>, Jie Fang<sup>1\*</sup>, Hongjian Jin<sup>2</sup>, Beisi Xu<sup>2</sup>, Shivendra Singh<sup>1</sup>, Anoushka Mullasseril<sup>1</sup>,  
6 Victoria Jones<sup>1</sup>, Ahmed Abu-Zaid<sup>1</sup>, Xinyu von Buttlar<sup>1</sup>, Bailey Cooke<sup>1</sup>, Dongli Hu<sup>1</sup>, Jason Shohet<sup>3</sup>,  
7 Andrew J Murphy<sup>1</sup>, Andrew M Davidoff<sup>1</sup>, Jun Yang<sup>1</sup>

8

9 <sup>1</sup>Department of Surgery, <sup>2</sup>Center for Applied Bioinformatics, St. Jude Children's Research Hospital, 262  
10 Danny Thomas Place, Memphis, TN 38105

11 <sup>3</sup> Department of Pediatrics, University of Massachusetts Medical School, 55 Lake Avenue North,  
12 Worcester, MA 01655

13 \*equal contribution

14

15 Correspondence: Jun.Yang2@stjude.org or Andrew.Davidoff@stjude.org

16

17

18

19

20

21

22

23

24

25

26

27

28

29

30

31

32

33

34 **ABSTRACT**

35 The H3K27me2/me3 histone demethylase KDM6B is over-expressed in neuroblastoma and is essential to  
36 neuroblastoma cell survival. While the KDM6B inhibitor, GSK-J4, has shown activity in *in vitro* and *in*  
37 *vivo* preclinical models, the mechanism of action remains poorly defined. We demonstrate that genetic  
38 and pharmacologic inhibition of KDM6B downregulates the pRB-E2F transcriptome and *MYCN*  
39 expression. Chemical genetic analyses show that high expression of the E2F transcriptome is positively  
40 correlated with sensitivity of cancer cells to GSK-J4. Mechanistically, inhibition of KDM6B activity 1)  
41 reduces the chromatin accessibility of E2F target genes and *MYCN*, 2) selectively leads to an increase of  
42 H3K27me3 but a decrease of the enhancer mark H3K4me1 at the CTCF and BORIS binding sites, which  
43 may, consequently, disrupt the long-range chromatin interaction of *MYCN* and E2F target genes, and 3)  
44 phenocopies the transcriptome induced by the specific CDK4/6 inhibitor palbociclib. Overexpression of  
45 CDK4/6 or *Rb1* knockout confers neuroblastoma cell resistance to both palbociclib and GSK-J4. A gene  
46 signature targeted by KDM6B inhibition is associated with poor survival of patients with neuroblastoma  
47 regardless of the *MYCN* status. These data indicate that KDM6B activity promotes an oncogenic CDK4/6-  
48 pRB-E2F pathway in neuroblastoma cells via H3K27me3-dependent enhancer-promoter interactions,  
49 providing a rationale to target KDM6B for high-risk neuroblastoma.

50  
51 Key words: KDM6B, MYC, E2F, Neuroblastoma, CDK4/6, Palbociclib

52  
53  
54  
55  
56  
57  
58  
59  
60  
61  
62  
63  
64  
65

## 66 INTRODUCTION

67 KDM6 is a Jumonji domain-containing H3K27me3/me2 demethylase subfamily<sup>1-4</sup> that antagonizes the  
68 activity of polycomb repressive complex 2 (PRC2)<sup>5</sup>, the methyltransferase of H3K27. KDM6 consists of  
69 3 members, KDM6A, KDM6B and UTY, although UTY has low lysine demethylase activity<sup>6</sup>. While  
70 KDM6A is believed to be a tumor suppressor and is mutated in many different types of cancer<sup>7,8</sup>, the  
71 function of KDM6B in cancer remains poorly defined. Early studies have shown that KDM6B contributes  
72 to activation of the *Ink4a/Arf* locus in fibroblasts in response to oncogenic stress<sup>9,10</sup>, and nuclear p53  
73 protein stabilization in glioblastoma cells<sup>11</sup>. Loss of KDM6B enhances aggressiveness of pancreatic  
74 cancer cells<sup>12</sup>. These data suggest KDM6B might have a tumor suppressive function. However, KDM6B  
75 is overexpressed in various cancers<sup>13</sup>, indicating that KDM6B may play different roles depending on the  
76 cellular context. KDM6B appears to be essential for the initiation and maintenance of NOTCH-driven  
77 acute T-cell lymphoblastic leukemia<sup>14</sup>, regulates multiple myeloma cell growth and survival by  
78 modulating the MAPK pathway<sup>15</sup>, drives glioblastoma stem cell plasticity and drug tolerance by  
79 chromatin remodeling<sup>16</sup>, and promotes migration, invasion, and stem cell-like behaviors in hepatocellular  
80 carcinoma<sup>17</sup>. KDM6B is also involved in chemotherapy resistance<sup>18</sup>.

81 Neuroblastoma, the most common extra-cranial solid tumor in children, arises as a result of  
82 blocked differentiation of neural crest precursors (NCCs) during development of the sympathetic nervous  
83 system<sup>19,20</sup>. This aggressive malignancy accounts for 15% of cancer-related deaths in children<sup>21</sup>. Although  
84 outcomes for children with low- or intermediate-risk disease are excellent, fewer than 50% of children  
85 with high-risk disease survive despite aggressive multimodal therapy. In patients with high-risk disease,  
86 one key biological feature associated with poor prognosis is amplification of the *MYCN* oncogene  
87 (MNA)<sup>22</sup>. As a master lineage transcription factor that drives tumorigenesis, the functions of *MYCN* have  
88 been associated with targetable epigenetic modifiers<sup>23-25</sup>. Our previous study demonstrated that the histone  
89 demethylase KDM4B regulates *MYC* activity and promotes tumor growth and maintenance of  
90 neuroblastoma<sup>26</sup>. More recently, we identified a novel KDM4B inhibitor ciclopirox<sup>27</sup>, that inhibits tumor  
91 growth and promotes differentiation<sup>27</sup>. *EZH2*, the essential catalytic unit of the PRC2 complex, is a  
92 *MYCN* target that represses neuronal differentiation in a H3K27me3-dependent manner, leading to  
93 inactivation of a tumor suppressive program in neuroblastoma<sup>28</sup>.

94 In this study, we show that KDM6B is highly expressed in neuroblastoma and its genomic locus  
95 is broadly marked with transcriptionally active histone modifications and transcription factor binding.  
96 Using chemical genetic and epigenetic approaches, we show that KDM6B is involved in regulation of the  
97 key oncogenic CDK4/6-pRB-E2F pathway and expression of both *MYCN* and *C-MYC* proto-oncogenes.

98 Furthermore, the E2F transcriptome serves as a biological marker of KDM6 inhibitor sensitivity.  
99 Pharmacological inhibition of KDM6B activity alters the chromatin accessibility of E2F target genes and  
100 *MYCN*, induces the redistribution of H3K27me3 and the enhancer mark H3K4me1. We propose that this  
101 may disrupt the long-range chromatin interaction of the E2F transcriptome within the same topologically  
102 associated domains (TAD). At the level of transcriptome, KDM6B inhibition mimics the CDK4/6  
103 inhibitor palbociclib. Cancer cells resistant to CDK4/6 inhibitor also are resistant to KDM6B inhibition.  
104 The gene signature targeted by KDM6 inhibition was associated with poor patient survival. Thus, our  
105 studies reveal that KDM6B regulates the oncogenic CDK4/6-pRB-E2F pathway in *MYCN*-amplified  
106 neuroblastoma, revealing a new mechanism of regulation of the E2F transcriptome by an epigenetic  
107 modulator.

108

## 109 RESULTS

### 110 ***KDM6B* is highly expressed in human neuroblastoma and is associated with a transcriptionally** 111 **active epigenetic landscape**

112 We have previously shown that KDM6B, but not KDM6A or UTY, is essential for neuroblastoma cell  
113 survival<sup>27</sup>. To more clearly define the role of KDM6B in neuroblastoma, we first compared expression of  
114 KDM6 family genes in normal trunk neural crest-derived tissues, neuroblastoma being a neural crest-  
115 derived cancer of the peripheral nervous system<sup>29</sup>, with expression in tumors in 4 different neuroblastoma  
116 patient cohorts<sup>30-32</sup>. While expression of *KDM6A* and *UTY* did not show consistent differences in tumors  
117 as compared to normal tissue of neural crest origin, *KDM6B* expression was significantly elevated across  
118 all 4 neuroblastoma cohorts ( $p < 0.001$ ) (Figure 1A-1C). We also found that levels of *KDM6B* expression,  
119 but not *KDM6A* or *UTY*, in neuroblastoma cell lines were among the highest, across 40 different cancer  
120 lineages (Supplementary Figure 1A). Analysis of the data from 15 subtypes of pediatric cancers (PCGP  
121 project performed at St Jude) also showed *KDM6B* expression was among the highest in neuroblastoma  
122 (Supplementary Figure 1B). We then compared the RNA-seq transcript counts of *KDM6B*, *KDM6A* and  
123 *UTY* in three large neuroblastoma cohorts and found that expression of *KDM6B* was significantly higher  
124 than that of *KDM6A* or *UTY* (Figure 1D-1F).

125 Gene transcription status is usually associated with a distinct epigenetic landscape. For example,  
126 high levels of H3K4me1, H3K4me3 and H3K27Ac are marks of active gene transcription while high  
127 levels of H3K27me3 and H3K9me3 are marks of repressive gene transcription<sup>33</sup>. To determine whether  
128 high expression of KDM6B in neuroblastoma is associated with active epigenetic modifications, we  
129 investigated the epigenetic landscapes at the genomic loci of *KDM6B*, *KDM6A* and *UTY* in 7 primary



130 human neuroblastoma tissues sequenced at St Jude, 4 with MNA and 3 without MNA (Figure 1G,  
131 Supplementary Figure 2). Regardless of the *MYCN* status, the genomic locus of *KDM6B* across 22-kb in  
132 length in all 7 human neuroblastoma cell lines is occupied by RNA polymerase II, which drives gene  
133 transcription, in accordance with enrichment of active gene transcription marks H3K4me1, H3K4me2,  
134 H3K4me3, H3K27Ac, H3K9-K14Ac, and H3K36me3. However, no transcriptionally repressive  
135 H3K27me3 or H3K9me3 marks were occupied at the *KDM6B* locus. The broad occupation of H3K4me1  
136 and H3K27Ac across the whole locus of *KDM6B* indicates that a super-enhancer<sup>34,35</sup> may regulate the  
137 expression of *KDM6B* in neuroblastoma. In contrast, the epigenetic landscapes at the *KDM6A* and *UTY*  
138 loci appeared to lack transcriptionally active gene transcription marks (Figure 1G, Supplementary Figure  
139 2). The promoter region and gene body of *KDM6A* were occupied by the transcriptionally repressive marks  
140 H3K27me3 and H3K9me3, respectively. In summary, *KDM6B* is highly expressed in human  
141 neuroblastoma and its genomic locus is epigenetically modified for active gene transcription, which is  
142 distinct from its paralogs *KDM6A* and *UTY*.

143

#### 144 **KDM6B regulates MYC expression**

145 We further validated the importance of KDM6B in neuroblastoma by assessing colony formation after  
146 knocking down *KDM6B* with 4 different siRNAs in BE2C cells (with MNA) and SK-N-AS cells (with  
147 high C-MYC activity). KDM6B depletion greatly reduced colony formation in both neuroblastoma cell  
148 lines, and was correlated with the KDM6B knockdown efficiency (Figure 1H,1I), consistent with our  
149 previous study<sup>27</sup>. In support of our data, neuroblastoma is the third most sensitive among 25 different  
150 cancer lineages that are sensitive to knockdown of KDM6B but not KDM6A (Supplementary Figure 3A,  
151 3B), just below prostate cancer and myeloma, in a genome-wide shRNA screen (20 shRNAs per gene) in  
152 709 cancer cell lines (DepMap dataset). Notably, depletion of KDM6B led to *MYCN* and C-MYC  
153 reduction in neuroblastoma cells (Figure 1I, Supplementary Figure 3C-F). Importantly, introduction of  
154 retroviral based KDM6B cDNA without its endogenous 3'UTR rescued the colony formation and *MYCN*  
155 expression in BE2C cells when endogenous KDM6B was depleted using a siRNA designed to target its  
156 3'UTR (Figure 1J-L), demonstrating the phenotype induced by KDM6B depletion is not due to an off-  
157 target effect. Conversely, overexpression of KDM6B in BE2C cells reduced H3K27me3, increased  
158 *MYCN* expression and promoted cell proliferation (Supplementary Figure 3G, H). Additionally, we found  
159 that KDM6B also regulated *MYC* expression in other cancer lineages such as lung cancer, osteosarcoma,  
160 and colorectal cancer cells and that this was independent of p53 status (Supplementary Figure 3I-L). These  
161 data indicate that KDM6B is needed for *MYC* expression in cancer cells.

162

### 163 **KDM6B regulates a pRB-E2F transcription program in neuroblastoma**

164 To investigate the molecular function of KDM6B in neuroblastoma, we performed RNA-seq followed by  
165 gene set enrichment analysis (GSEA) after knockdown of KDM6B in MYCN-amplified (BE2C and  
166 KELLY) and MYCN-non-amplified cells (SK-N-AS, SK-N-FI). Strikingly, GSEA results showed that  
167 the top hits of KDM6B downstream targets were enriched with E2F gene sets, *Rb1* knockout signatures  
168 (*Rb1* encodes pRB, is a negative regulator of E2F activity<sup>36</sup>) and other cell cycle gene signatures (Figure  
169 2A-2C, Supplementary Figure 4A, 4B), in the two MYCN amplified cell lines. Motif analysis of the  
170 KDM6B target genes also revealed that they were mainly enriched with E2F binding motifs (Table 1).  
171 These data indicate that KDM6B regulates the transcriptome of the E2F pathway in MYCN-amplified  
172 neuroblastoma cells. The E2F transcription factors are critical regulators of cell cycle progression by  
173 directly regulating more than 100 genes including those encoding cyclins<sup>37</sup>. Early studies showed that E2F  
174 also binds to promoters of *C-MYC* and *MYCN* to regulate their expression<sup>38,39</sup>. GSEA data revealed that  
175 MYC targets were also significantly downregulated by KDM6B depletion (Figure 2A). Interestingly, the  
176 top signatures upregulated by KDM6B knockdown in SK-N-FI were enriched with E2F gene sets  
177 (Supplementary Figure 4C, 4D), although C-MYC expression was reduced (Supplementary Figure 3F).  
178 However, the E2F gene signatures were less affected in SK-N-AS cells than BE2C, KELLY and SK-N-  
179 FI although one E2F3 gene set was downregulated by KDM6B knockdown (Supplementary Figure 3E,  
180 3F).

181 We further investigated KDM6B function using pharmacologic inhibition. GSK-J1 is the only  
182 selective KDM6 inhibitor available<sup>40</sup>, but, unfortunately, it is unable to penetrate cells. To make GSK-J1  
183 cell-permeable, GSK-J1 was modified by adding an ester (new reagent was named GSK-J4)<sup>40</sup>. Thus, GSK-  
184 J4 is not itself a chemical tool for direct KDM inhibition, but was designed specifically to enable efficient  
185 intracellular delivery of GSK-J1 into cells. The intracellular conversion of the ester pro-drug is complete  
186 within 15 min after which levels of intracellular GSK-J4 are negligible<sup>41</sup>. Once entering cells, GSK-J4  
187 converts back to GSK-J1, consequently inhibiting KDM6 (Supplementary Figure 5A)<sup>40</sup>. To validate this  
188 and profile the selectivity of GSK-J1/GSK-J4, we used an AlphaLISA approach, a method that tests the  
189 *in vitro* inhibitory activity of GSK-J1 and GSK-J4 against purified KDMs (KDM2A, KDM3A, KDM4A,  
190 KDM5A, KDM6A, KDM6B). We confirmed that GSK-J1 was selectively effective against KDM6A and  
191 KDM6B, had some effect on KDM5A but showed no activity against KDM2A, KDM3A and KDM4A  
192 (Supplementary Figure 5B), a result consistent with published GSK data<sup>40</sup>. However, GSK-J4 showed no  
193 *in vitro* activity against all tested KDMs (Supplementary Figure 5C). While GSK-J4 could have off-target

194 effects when administered at high concentrations, the concentration we used in cells (2.5  $\mu$ M) only induced  
195 the upregulation of H3K27me3, but not H3K9me3, H3K36me3 and H3K4me3 (Supplementary Figure  
196 5D), three other major histone methylation sites of H3, indicating that GSK-J4 induced its cellular effect  
197 by selectively targeting KDM6 but not other KDMs. Additionally, a selective KDM5 inhibitor, KDM5-  
198 C70<sup>42</sup>, showed no effect on neuroblastoma cell proliferation even when administered at very high  
199 concentrations (40 $\mu$ M) (Supplementary Figure 5E, 5F).

200 Treatment of neuroblastoma cells and normal human fibroblasts (HS68) with GSK-J4, in a colony  
201 formation assay, showed that GSK-J4 inhibited colony formation in a concentration-dependent manner,  
202 with a significant effect observed in the majority of cell lines at concentrations of 1.0-2.0 $\mu$ M  
203 (Supplementary Figure 6A). However, HS68 cells were unaffected by GSK-J4. Consistent with these  
204 results, another recent study showed that GSK-J4 has a potent effect on neuroblastoma cell survival<sup>43</sup>. To  
205 define the molecular mechanism of GSK-J4 action on neuroblastoma cells, we performed global gene  
206 expression profiling for GSEA analysis after GSK-J4 treatment of BE2C cells. GSK-J4 induced a very  
207 similar transcriptome profile as depletion of KDM6B and the gene sets most significantly downregulated  
208 by this inhibitor were enriched with cell cycle, *Rbl* knockout and E2F pathways (Figure 2D-2F).  
209 Transcription factor motif binding analysis showed that genes downregulated by GSK-J4 were greatly  
210 enriched with E2F binding (Table 2). Again, MYCN and C-MYC expression were also downregulated by  
211 GSK-J4 treatment (Supplementary Figure 6B-6D), consistent with KDM6B depletion (Supplementary  
212 Figure 3). Re-analysis of an independent RNA-seq data set<sup>43</sup> also showed that KDM6 inhibition led to  
213 downregulation of gene sets enriched with *Rbl* knockout and DREAM complex (dimerization partner,  
214 RB-like, E2F and multi-vulval class B) in neuroblastoma cells (Supplementary Figure 7). Thus, GSK-J4  
215 phenocopied KDM6B depletion in neuroblastoma cells and, therefore, its therapeutic effect may be  
216 mediated through inhibition of KDM6B. Taken together, genetic and pharmacologic inhibition of  
217 KDM6B predominantly leads to downregulation of the pRB-E2F transcriptional program, particularly in  
218 MYCN-amplified neuroblastoma cells.

219

## 220 **Pharmacogenetics reveals that the E2F transcriptome is associated with sensitivity to KDM6B** 221 **inhibition**

222 While the presence of KDM6B is a prerequisite for GSK-J4 activity in neuroblastoma cells<sup>43</sup>, expression  
223 levels of KDM6B do not correlate with GSK-J4 sensitivity<sup>43</sup>. A biomarker that predicts therapy response  
224 is critical for patient stratification. Since KDM6B inhibition appears to effect its anti-tumor activity  
225 through downregulation of the E2F transcriptome, we hypothesized that high levels of the E2F

226 transcriptome may correlate with the response of cancer cells to KDM6B inhibition. The gene signatures  
227 induced by chemical (i.e., small-molecule) or genetic perturbations (i.e., siRNA knockdown) can be used  
228 to connect unknown mechanisms of action (MoA) of chemical probes. Differential gene expression has  
229 been correlated with patterns of small-molecule sensitivity across many cell lines to illuminate the actions  
230 of compounds whose MoA are unknown<sup>44,45</sup>. The Cancer Therapeutic Response Portal correlated the  
231 sensitivity patterns of 481 compounds including GSK-J4 with 19,000 basal transcript levels across 823  
232 different human cancer cell lines and identified selective outlier transcripts<sup>44,45</sup>, which allowed us to  
233 interrogate whether the KDM6B inhibitor activity was correlated with specific transcripts. The E2F genes  
234 such as *E2F8* were the ones most significantly affected by KDM6B inhibition (Figure 2). *E2F8* is an  
235 atypical E2F and downstream target of E2F1-3<sup>46</sup>. We chose *E2F8* as a representative gene to correlate  
236 E2F pathway activity with drug effect. Strikingly, GSK-J4 ranked highest among the top compounds  
237 whose cellular activity was correlated with *E2F8* expression (Pearson correlation  $R=-0.528$ , z-score = -  
238 4.56, Figure 3A). We arbitrarily chose 13 cell lines with high *E2F8* expression as group A, and 8 cell lines  
239 with low *E2F8* expression as group B, which had high sensitivity and low sensitivity to GSK-J4,  
240 respectively (Figure 3B, Supplementary Table 1). We then used GSEA to infer the pathways that differed  
241 in the two groups. We found that the pRB-E2F gene sets were the most significant hits in group A cell  
242 lines (Figure 3C, 3D). The genes highly expressed in group A cells were profoundly enriched with E2F  
243 transcription factor binding motifs (Supplementary Table S2), and most of the top 50 genes such as *E2F1*  
244 and *E2F8* are involved in regulation of the cell cycle (Supplementary Figure 8A). MYC signatures were  
245 also enriched in group A cells (Supplementary Figure 8B-8D). We also selectively investigated several  
246 other E2F genes including *ASF1B*, *CDK2* and *E2F1*, all of which were positively correlated with GSK-J4  
247 sensitivity (Supplementary Figure 8E-8G). Therefore, cancer cells with high E2F activity appear to be  
248 more sensitive to KDM6B inhibition.

249 To specifically investigate the conclusion that high E2F activity serves as a biomarker for sensitivity  
250 to KDM6B inhibition in neuroblastoma, we categorized neuroblastoma cell lines into two groups  
251 according to their  $IC_{50}$  to GSK-J4<sup>43</sup>. GSEA analysis of RNA-seq data of these cell lines showed a very  
252 similar transcriptome pattern to KDM6B knockdown or GSK-J4 inhibition for those with lower  $IC_{50}$  to  
253 GSK-J4 (more sensitive), which were enriched with E2F and MYC gene signatures (Figure 3E). For  
254 example, SK-N-FI cells with high E2F transcriptome expression were more sensitive to GSK-J4 than SK-  
255 N-SH cells (Figure 3F), which had lower expression of the E2F transcriptome. The genes highly expressed  
256 in neuroblastoma cells that were more sensitive to GSK-J4 were predominantly enriched with E2F  
257 transcription factor binding motifs (Table 3). Taken together, these data demonstrate that a high E2F gene

258 signature is correlated with GSK-J4 sensitivity, and thus it may serve as a biomarker for effectiveness of  
259 KDM6B inhibitors in cancer treatment in the future. These data also further support that KDM6B regulates  
260 the E2F transcriptome.

261

### 262 **Inhibition of KDM6B activity reduces the chromatin accessibility of E2F target genes and *MYCN***

263 To understand how KDM6B regulates the E2F pathway, we performed Assay for Transposase-Accessible  
264 Chromatin with high-throughput sequencing (ATAC-seq) after 24h and 48h of GSK-J4 treatment, for  
265 mapping genome-wide chromatin accessibility<sup>47</sup>. The 24h GSK-J4 treatment resulted in upregulation of  
266 8386 nucleosome-free, open chromatin regions (log<sub>2</sub> fold change  $\geq 0.5$ ,  $p < 0.05$ , Figure 4A), 46.9% of  
267 which were located at the annotated promoter regions (within 2-kb from transcription start site, TSS) and  
268 39% of which were located at the annotated enhancer regions (2-50kb distance from TSS). The rest  
269 (14.1%) were located at more distal regions. However, 9574 nucleosome free, open chromatin regions  
270 were downregulated by GSK-J4 treatment (Figure 4A), only 18.5% of which were located at the promoter  
271 regions and 61.8% of which were located at enhancer regions, while 19.7% were located at more distal  
272 regions. The 48h GSK-J4 treatment further enhanced its effect on DNA accessibility, resulting in an  
273 increase of 13546 and decrease of 11027 peaks, respectively (Figure 4A). The proportions of the annotated  
274 regions tended to be similar to that of 24h treatment. Among the regions with upregulated chromatin  
275 accessibility, 57.6% were located at promoter regions, 29.5% were located at enhancer regions, and 12.9%  
276 were located at more distal regions (Figure 4A). Among the regions with downregulated chromatin  
277 accessibility, 17.9% were located at promoter regions and 57.8% were located at enhancer regions, while  
278 24.3% were located at more distal regions (Figure 4A). We further assessed whether altered chromatin  
279 accessibility was associated with changes in gene expression. Indeed, the genes annotated with differential  
280 accessibility regions (DARs) at promoters or enhancers were significantly enriched in differentially  
281 expressed genes by GSK-J4 treatment (Supplementary Figure 9). For example, DNA accessibility at the  
282 promoter region of the oncogene *AKT1* was reduced by GSK-J4, and one additional peak at a potential  
283 enhancer region near the long non-coding RNA *LINC00638* was also decreased (Figure 4B). The  
284 reduction of chromatin accessibility was consistent with the reduced expression of *AKT1* transcripts.  
285 *AKT1* is a key molecule in the PI3K-mTOR pathway<sup>48</sup>, and E2F upregulates AKT activity through a  
286 transcription-dependent mechanism<sup>49</sup>. *E2F8*, whose expression was downregulated by KDM6B  
287 knockdown and GSK-J4 treatment, did not show significant changes in DNA accessibility within its  
288 promoter region. However, several peaks at the distal region of *E2F8* which extended to the adjacent  
289 *NAV2* locus were altered by GSK-J4 (Figure 4C). Notably, our RNA-seq analysis showed that the *NAV2*



290 locus is not expressed in BE2C cells (Figure 4C). These data suggest that *E2F8* expression might be  
291 regulated by a distal enhancer that is silenced by KDM6B inhibition. Similarly, we did not observe  
292 significant changes at the promoter regions of *MYCN*, and cell cycle genes (*CCNE1*, *BUB1* and *BIRC5*);  
293 however, the DNA accessibility at the distal regions of these genes were reduced (Supplementary Figure  
294 10A-10D). The downregulation of gene expression by GSK-J4 was not always correlated with reduction  
295 of DNA accessibility. For example, chromatin accessibility at the *AURKB* promoter was increased by  
296 GSK-J4 although its transcript expression was reduced (Supplementary Figure 10E), suggesting that the  
297 open chromatin may recruit transcription suppressors to repress its gene transcription. For *CDKN1A*,  
298 which encodes p21 to inhibit the CDK2/Cyclin E complex during S phase of the cell cycle, the DNA  
299 accessibility at its promoter and enhancer regions was enhanced, consistent with its transcript induction  
300 by KDM6B inhibition (Supplementary Figure 10F).

301 Transcription factor motif analysis of the ATAC-seq data using genomic footprinting  
302 demonstrated that E2F binding motifs had reduced DNA accessibility (Figure 4D, 4E). Downregulated  
303 open chromatin regions were also observed for MYCN and MYC/MAX binding motifs (Figure 4E). These  
304 data indicate that KDM6B inhibition impacts the chromatin accessibility and transcription of E2F and  
305 MYC pathway genes.

306

### 307 **KDM6B inhibition induces an increase of H3K27me3 but a decrease of the enhancer mark** 308 **H3K4me1 at CTCF and BORIS binding sites**

309 To examine the impact of KDM6B inhibition on epigenetic marks, we performed Cleavage Under Targets  
310 & Tagmentation (CUT&Tag) to assess the alterations of H3K27me3, the KDM6B substrate, and  
311 H3K4me1, the enhancer mark, after KDM6B knockdown and GSK-J4 treatment of BE2C cells.  
312 CUT&Tag is an epigenomic profiling strategy that overcomes shortcomings of ChIP-seq<sup>50</sup>. In CUT&Tag,  
313 the H3K27me3 and H3K4me1 were bound in situ by specific antibodies, which were then tethered to a  
314 protein A-Tn5 transposase fusion protein. Activation of the transposase efficiently generates fragment  
315 libraries with high resolution and exceptionally low background<sup>50</sup>. The CUT&Tag library size for each  
316 sample was adjusted by *E. Coli* residual genomic DNA as a spike-in scaling factor, which was used to  
317 normalize the read counts for the downstream differential analysis. KDM6B inhibition induced a modest  
318 increase of global H3K27me3 peaks (Supplemental Table 3, Supplemental Figure 11A). We specifically  
319 assessed the H3K27me3 in the differentially expressed genes induced by KDM6B inhibition. Among the  
320 genes differentially regulated by KDM6B knockdown and GSK-J4 treatment, the patterns of H3K27me3  
321 changes tended to be similar in both groups (Figure 5A), suggesting that GSK-J4 mainly acts through

322 KDM6B to modulate the H3K27me3 levels. In particular, the H3K27me3 signals at the super-enhancer  
323 region of *MYCN* (the genomic region between *MYCN* and *FAMI49A*, with a noncoding RNA *GACAT3*  
324 between both of them<sup>23,51</sup>) were most significantly upregulated by KDM6B knockdown or GSK-J4  
325 treatment (Figure 5C, Supplemental Figure 11A), which is consistent with the downregulation of *MYCN*  
326 by KDM6B inhibition. We further assessed H3K4me1, the enhancer mark, using CUT&Tag after KDM6B  
327 knockdown and GSK-J4 treatment (Supplemental Table 4). Similar patterns of H3K4me1 changes were  
328 observed in both groups (Figure 5B). Interestingly, while more peaks of H3K4me1 were increased in  
329 genes downregulated by KDM6B inhibition, the super-enhancer region of *MYCN* showed most significant  
330 downregulation of H3K4me1 although GSK-J4 also induced an increase of several peaks at this region  
331 (Figure 5C, Supplemental Figure 11B), suggesting that *MYCN* super-enhancer region is particularly  
332 susceptible to perturbation of KDM6B inhibition.

333 The alterations of H3K27me3 and H3K4me1 by KDM6B inhibition mainly occurred at non-  
334 promoter regions (Supplemental Figure 11C), suggesting that KDM6B has a major impact on distal  
335 regulatory elements of transcription. Transcriptional factor motif analyses of H3K27me3 and H3K4me1  
336 peaks revealed that KDM6B inhibition dominantly led to an increase of H3K27me3 but a decrease of  
337 H3K4me1 at the CTCF and BORIS binding sites (Figure 5D, E), and no enrichment with *MYCN* or E2F  
338 binding sites. CTCF and BORIS (also named CTCFL) play an important role in chromatin looping and  
339 long-range chromatin interactions<sup>52-54</sup>. H3K4me1 is an essential feature of enhancers and is bound by  
340 multiple chromatin-associated factors such as BAF complex and Cohesion<sup>55</sup>, which facilitate enhancer-  
341 promoter looping<sup>56,57</sup>. Since the majority of upregulated H3K27me3 peaks were located at distal  
342 regulatory regions, we hypothesized that the H3K27me3 changes at these distal regions repressed  
343 transcription of *MYCN* and E2F target genes via alteration of chromatin structure and enhancer/promoter  
344 interactions. To investigate this possibility, we cross-referenced the Hi-C chromatin conformation of  
345 BE2C cells. Interestingly, *MYCN* is located at the same topologically associated domain (TAD) as the  
346 *GACAT3* and *FAMI49A* loci, marked as a super-enhancer by broad H3K27Ac occupancy, showing  
347 dysregulated H3K27me3 and H3K4me1 by KDM6B inhibition (Figure 5C). A TAD domain is a self-  
348 interacting genomic region that regulates gene expression by limiting the enhancer-promoter interaction  
349 to each TAD<sup>58,59</sup>. Chromatin interaction was observed across this region (Figure 5F), supporting the  
350 hypothesis that KDM6B inhibition may disrupt the chromatin interaction, leading to reduced transcription  
351 of *MYCN*. Similarly, we found the *E2F8* gene locus showed multiple chromatin interactions with adjacent  
352 genes within the TAD, particularly to the *NAV2* locus (Supplemental Figure 11D, E). Taken together,

353 these data suggest that KDM6B inhibition might alter the long-range interactions of *MYCN* and E2F target  
354 genes in TAD, repressing the *MYCN* and E2F regulated transcriptome.

### 355 **GSK-J4 reduces the expression of the PRC2 complex**

356 The homeostasis of H3K27me3 is balanced by PRC2 and KDM6<sup>5</sup>. More H3K27me3 peaks were expected  
357 by KDM6 inhibition. However, GSK-J4 treatment did not lead to expected high number loci of  
358 H3K27me3 (Supplemental Figure 11A). To explain this discrepancy, we examined the expression of the  
359 PRC2 complex. The key PRC2 components (EZH2, SUZ12 and EED) have been shown to be pRB-E2F  
360 targets<sup>60,61</sup>. Consistent with the data that KDM6B inhibition mainly downregulated an pRB-E2F  
361 transcriptome, GSK-J4 treatment indeed reduced the expression of the PRC2 complex (Supplementary  
362 Figure 12A), However, the expression of global H3K27me3 was minimally affected, indicating that the  
363 expected H3K27me3 upregulation by KDM6 inhibition is counterbalanced by reduced expression of  
364 PRC2. A recent study identified a 37-gene signature of EZH2<sup>28</sup>, which is repressed by EZH2 and silenced  
365 in *MYCN*-amplified high-risk neuroblastoma. GSEA analysis revealed that this 37-gene signature was  
366 significantly associated with the GSK-J4 treatment (Supplementary Figure 12B, 12C), suggesting that  
367 KDM6B inhibition consequently downregulates the functions of PRC2, leading to the induction of tumor-  
368 suppressive program repressed by EZH2.

369

### 370 **Inhibition of KDM6B mimics CDK4/6 inhibitor Palbociclib**

371 To further investigate the biological functions of KDM6B, we integrated the KDM6B downstream target  
372 genes with information from the Library of Integrated Network-Based Cellular Signatures (LINCS) data.  
373 LINCS data is composed of tens of thousands of gene sets, indicative of the transcriptional responses to a  
374 large library of chemical compounds<sup>62</sup>. With this approach, we found that genes downregulated by  
375 KDM6B knockdown in neuroblastoma cells (Supplementary Table S5) overlapped significantly with the  
376 transcriptomes downregulated by palbociclib (Figure 6A), a specific CDK4/6 inhibitor that acts upstream  
377 of the E2F pathway in cell cycle regulation. Similarly, genes downregulated by GSK-J4 (Supplementary  
378 Table S6) also significantly overlapped the transcriptomes downregulated by palbociclib (Figure 6B).  
379 CDK4/6 inhibitor signatures being identified among the most correlated signatures with KDM6B  
380 knockdown or GSK-J4 treatment further demonstrated that KDM6B is mainly involved in regulation of  
381 the E2F pathway. To corroborate these findings, we treated 4 different neuroblastoma cell lines (2 with  
382 MNA and 2 without MNA) with palbociclib and performed RNA-seq for differential gene expression  
383 analyses. By comparing the genes most significantly downregulated by palbociclib among these cell lines  
384 via Venn program (Supplementary Figure 13), we extracted 89 common genes (Supplementary Table S7).



385 GSEA results showed that the 89-gene signature was significantly enriched within gene sets  
386 downregulated by KDM6B knockdown (Figure 6C) or GSK-J4 treatment (Figure 6D). Although single  
387 drug treatment effectively inhibited colony formation in a dose dependent manner, the combination of  
388 GSK-J4 and palbociclib did not enhance the inhibitory effect on colony formation of BE2C cells, as shown  
389 by colony formation and Bliss combination index (Figure 6E, 6F), likely because both drugs target the  
390 same pathway. However, GSK-J4 greatly enhanced the effect of 17-DMAG, an HSP90 inhibitor  
391 (Supplementary Figure 14A, 14B), and JQ-1, a bromodomain inhibitor that targets BRD4<sup>63</sup>  
392 (Supplementary Figure 14C, 14D). Interestingly, we observed some degree of synergy of GSK-J4 and  
393 palbociclib, as well as 17-DMAG and JQ-1 in SK-N-AS cells (Supplementary Figure 14E-G), the non-  
394 MYCN amplified cells with less impact on E2F pathways by KDM6B inhibition.

395

#### 396 **Cancer cells with acquired CDK4/6 inhibitor resistance are less responsive to GSK-J4**

397 Upon mitogen stimulation, CDK4 and CDK6 phosphorylate the pRB protein, leading to release of E2F  
398 transcription factors from pRB for gene transcription<sup>64</sup>. CDK4/6 inhibitors including palbociclib showed  
399 promising efficacy in ER<sup>+</sup>/HER2<sup>-</sup> breast cancer and have been approved for clinical use<sup>65,66</sup>. Over 100  
400 clinical trials of CDK4/6 inhibitors for a variety of cancers are currently in progress<sup>65</sup>. However, acquired  
401 resistance to CDK4/6 inhibitors, as observed during breast cancer treatment, is expected and the  
402 mechanism involves amplification of *CDK6* or loss of function of *Rb1*<sup>65,66</sup>. To test if these mechanisms  
403 also diminish the effect of GSK-J4, we transduced the BE2C cells with lentiviral based CDK4 and CDK6  
404 (Figure 6G). Overexpression of CDK4 or CDK6 conferred expected resistance in neuroblastoma cells to  
405 palbociclib, as shown by colony formation and EC50 shift (Figure 6H, I). Cells which overexpressed  
406 CDK4 or CDK6 also gained resistance to GSK-J4, although a higher concentration of GSK-J4 at 2.5 $\mu$ M  
407 was still able to kill them (Figure 6H, 6J). We then generated an *Rb1* knockout cell line for testing the  
408 response to GSK-J4 and palbociclib (Figure 6K). As expected, loss of *Rb1* conferred resistance to  
409 palbociclib (Figure 6L). Similarly, the *Rb1* knockout cells were also resistant to GSK-J4 treatment in  
410 comparison with the *Rb1* wildtype cells (Figure 6M). Similar to the CDK4 or CDK6 overexpressing cells,  
411 the combination of palbociclib and GSK-J4 was not synergistic (Figure 6M). These data further  
412 demonstrate that KDM6B acts on the same pathway as pRB-E2F in neuroblastoma.

413

#### 414 **A gene signature targeted by KDM6B inhibition is associated with poor outcome**

415 To correlate the clinical relevance of target genes of KDM6B inhibition, we identified a 149-gene  
416 signature (Supplementary Table 8) that was commonly downregulated by GSK-J4 in BE2C and three

417 other neuroblastoma cell lines (IMR5, LAN5 and SK-N-FI)<sup>43</sup>. Among these 149 genes, 85 were highly  
418 expressed in the high-risk neuroblastomas while 20 were highly expressed in the low-risk neuroblastomas  
419 (Supplementary Table 9). Based on the expression levels of these differentially expressed genes in  
420 neuroblastomas, they were categorized into 4 clusters (Figure 7A). Cluster 3 and 4 neuroblastomas  
421 expressed higher levels of the GSK-J4 signature, and were enriched with high-risk, high-stage and  
422 MYCN-amplified tumors. While patients in clusters 1 and 2 showed excellent event-free and overall  
423 survival, clusters 3 and 4 patients had a significantly worse outcome (Figure 7B, 7C). No difference was  
424 observed between clusters 1 and 2. Cluster 4 showed a poorer survival than that of cluster 3, in line with  
425 the higher expression of GSK-J4 target genes in cluster 4. *MYCN* amplification (MNA) is a well-known  
426 poor prognostic risk factor in neuroblastoma. To investigate whether the correlation of the GSK-J4  
427 signature with patient outcome was affected by MNA status, we compared the event-free survival of  
428 clusters 3 and 4 with MNA. The results showed that cluster 4, which had higher levels of GSK-J4  
429 signature, was still correlated with a poorer event-free survival of patients with MNA although the overall  
430 survival was not statistically significant (Figure 7D, 7F). However, in stage 4 patients, cluster 4 showed  
431 significantly worse outcome in both event-free and overall survival than that of cluster 3 (Supplementary  
432 Figure 15). In high-risk patients, cluster 4 had a significantly worse outcome in event-free survival  
433 compared to cluster 3, but there was no difference in overall survival (Figure 7E, G). These data indicate  
434 that, in stage 4 or MNA patients, higher expression levels of the GSK-J4 signature is a high-risk factor.

435

436

## 437 **DISCUSSION**

438 Despite one recent study suggesting that KDM6B might be tumor suppressive in neuroblastoma<sup>67</sup>, we and  
439 others have found that KDM6B plays an important role in MYC-driven tumorigenesis and that  
440 pharmacologically targeting KDM6B by the small molecule GSK-J4 is therapeutically efficacious in  
441 multiple tumor models<sup>14,27,68-71</sup>, including high-risk neuroblastoma<sup>43</sup>. However, the anticancer  
442 mechanisms of KDM6B inhibition are poorly understood. Here we show that *KDM6B* is significantly  
443 over-expressed in human primary neuroblastoma in comparison with its paralogs *KDM6A* and *UTY*.  
444 Strikingly, the 22-kb genomic locus of *KDM6B* is heavily occupied by active gene transcription marks,  
445 including H3K4me1, H3K27Ac, BRD4 and RNA polymerase II binding while the *KDM6A* and *UTY* loci  
446 lack such histone modifications and transcription factor binding. These data explain why *KDM6B* is  
447 expressed at much higher levels than *KDM6A* and *UTY* in neuroblastoma. The long-distance broad marks  
448 at the KDM6B locus with H3K4me1 and H3K27Ac suggest *KDM6B* expression is under the control of a

449 super-enhancer, a large cluster of transcriptional enhancers that drive expression of genes that define cell  
450 identity<sup>72</sup>. We further found that KDM6B is predominantly involved in regulation of MYC expression and  
451 downstream target genes of the pRB-E2F pathway. Genetic and pharmacologic inhibition of KDM6B  
452 consistently repressed the expression of MYCN and C-MYC, and the transcriptome of E2F target genes.  
453 These results support previous studies demonstrating that E2F and MYC are functionally associated<sup>38,39</sup>,  
454 and that E2F drives MYC expression. MYC also regulates E2F expression and requires distinct E2F  
455 activities to induce S phase and apoptosis<sup>73</sup>. Moreover, a close association between E2F and MYC binding  
456 sites and their target genes has been observed<sup>74</sup>. Nevertheless, the impact of KDM6B inhibition on E2F  
457 pathways was more dramatic in MYCN-amplified neuroblastoma cells.

458 E2F deregulation in cancer often occurs through loss-of-function of the pRB tumor suppressor<sup>75</sup>.  
459 The E2F transcription factors (E2F1, E2F2, and E2F3a) bind at target gene promoters in complexes with  
460 their dimerization partner (DP1 or DP2) and pRB<sup>36</sup>, which suppresses target gene transcription through  
461 the recruitment of chromatin modifiers and remodeling factors such as HDAC and EZH2<sup>36,76</sup>. During the  
462 G1 phase of the cell cycle, oncogenes such as Ras induce D-type cyclins to activate cyclin dependent  
463 serine/threonine kinases CDK4 and CDK6, which phosphorylate pRB, consequently leading to release of  
464 E2F transcription factors from pRB, allowing for cell proliferation<sup>64</sup>. While *Rb1* loss is very rare in  
465 neuroblastoma, several studies have shown that the cyclin D/CDK4/CDK6 pathway is hyperactive in  
466 neuroblastoma<sup>77-82</sup>. Genome-wide CRISPR and shRNA screening demonstrated that knockout of *CDK4*  
467 or *CDK6* inhibited neuroblastoma cell proliferation/survival while *Rb1* knockout promoted cell  
468 proliferation (<https://depmap.org/portal/>). A majority of neuroblastoma models with MNA are sensitive  
469 to CDK4/6 inhibition<sup>83</sup>. These data indicate that the deregulated E2F pathway is essential to  
470 neuroblastoma. The genetic and pharmacologic KDM6B inhibition results in a predominant reduction of  
471 the E2F transcriptome and MYC, which may account for the therapeutic effect of KDM6B blockade in  
472 neuroblastoma. In addition, the transcriptome of KDM6B inhibition mimics the CDK4/6 inhibitor,  
473 palbociclib. When cells gained resistance to palbociclib by overexpressing CDK4/6 or by *Rb1* knockout,  
474 they also gained resistance to GSK-J4. Thus, these data further support that KDM6B regulates the  
475 CDK4/6-pRB-E2F pathway in neuroblastoma.

476 Intriguingly, while transcriptome, chemical genetics and ATAC-seq analyses show that  
477 KDM6B inhibition impacts MYCN and the E2F transcriptome, the loci of H3K27me3 alterations were  
478 not enriched with MYCN and E2F genes. As the majority of enhancer mark H3K4me1 and H3K27me3  
479 peaks altered by KDM6B inhibition were located at distal non-promoter regions, one possible explanation  
480 is that KDM6B inhibition disrupted the long-range chromatin interaction between its targets and the

481 regions with altered H3K27me3 and H3K4me1 because H3K4me1 functions to mediate the enhancer-  
482 promoter looping<sup>56,57</sup>. H3K4me1 is basically catalyzed by KMT2 family methyltransferases. Previous  
483 studies have shown that KMT2 members can form complexes with KDM6<sup>84-86</sup>, suggesting a concerted  
484 mechanism for transcriptional activation in which cycles of H3K4 methylation by KMT2 are linked with  
485 the demethylation of H3K27<sup>84-86</sup>. The transcriptional factor motif analysis showed that CTCF and BORIS  
486 binding motifs are the major sites impacted by altered H3K27me3 and H3K4me1. KDM6B inhibition  
487 specifically leads to increased H3K27me3 at CTCF and BORIS binding sites while H3K4me1 at CTCF  
488 and BORIS binding sites are selectively reduced. These data suggest that increased H3K27me3 displaces  
489 H3K4me1 modifiers (highly likely the H3K4me1 methyltransferase KMT2) from CTCF and BORIS sites,  
490 consequently disrupting the enhancer activity. Previous studies have shown that enhancers, CTCF and  
491 H3K4me1 peaks overlap<sup>87</sup>. CTCF regulates the long-range chromatin interactions at enhancers. Thus,  
492 KDM6B inhibition may disrupt the chromatin interaction at its target genes. *MYCN* and many E2F target  
493 genes reside in the same topologically associated domains (TAD) as the regions with elevated H3K27me3  
494 by KDM6B inhibition. TADs include chromatin loops that mediate promoter–enhancer contacts that  
495 regulate gene expression<sup>58,59</sup>. Our CUT&Tag data showed that the super-enhancer region of *MYCN*, which  
496 exhibits long-range chromatin interactions within a TAD domain, has the most significant changes of  
497 H3K27me3 and H3K4me1 by KDM6B knockdown and GSK-J4 treatment, in line with the reduction of  
498 *MYCN* expression by KDM6B inhibition. In erythroid cells, long-range control of epigenetic regulation  
499 has been observed in that KDM6B is recruited to the enhancer regions to erase H3K27me3, consequently  
500 evicting the gene silencing PcG protein for a high rate of transcription<sup>88</sup>. During early differentiation steps,  
501 the embryonic stem cell factor Tbx3 associates with KDM6B at the enhancer element of the *Eomes* locus  
502 to allow enhancer-promoter interactions<sup>89</sup>. This spatial reorganization of the chromatin primes the cells to  
503 respond to Activin signaling. In neural stem cells, SMAD3 recruits KDM6B at the enhancers in response  
504 to TGF- $\beta$ , for enhancer transcription<sup>90</sup>. Here we propose a model that, once stimulated by mitogens due  
505 to oncogenic activity, KDM6B is recruited to chromatin to maintain the low levels of H3K27me3 at the  
506 distal regulatory enhancer regions bound by CTCF and BORIS, which loops and physically interacts with  
507 E2F transcription factors that bind at the promoters of target genes, together with associated transcriptional  
508 machinery including RNA polymerase II and transcription mediators, driving the expression of *MYCN*  
509 and the E2F transcriptome (Figure 8A). When KDM6B is inhibited, the H3K27me3 accumulates at the  
510 distal regions and disrupts the assembly of transcriptionally active interaction of promoter-enhancers,  
511 leading to the downregulation of *MYCN* and the E2F transcriptome (Figure 8B).

512 Interestingly, expression of the PRC2 complex, which is a downstream target of pRB-E2F<sup>60,61</sup>  
513 and MYCN<sup>28</sup>, was downregulated by KDM6B inhibition, in line with of the decrease of a number of  
514 H3K27me3 peaks and de-repression of a tumor suppressive program governed by EZH2<sup>28</sup>. The connection  
515 between KDM6B and EZH2 is interesting. Since EZH2 is a downstream target of E2F and MYCN, we  
516 assumed the reduction of EZH2 by KDM6B inhibition is through this mechanism. However, considering  
517 both proteins are epigenetic modifiers that confer cellular plasticity, we also speculate that cells strive for  
518 adaptation to the KDM6B inhibition by suppressing EZH2 in order to counterbalance the net increase of  
519 H3K27me3.

520 Neuroblastoma is a disease that arises as a result of blocked differentiation of neural crest  
521 precursors (NCCs) during development<sup>19,20</sup>. EZH2 is required to maintain the undifferentiated state of  
522 neuroblastoma<sup>28,91</sup>. Thus, our data and that from other studies indicate that a network composed of MYCN,  
523 E2F, PRC2 and KDM6B regulates cell proliferation and differentiation of neuroblastoma (Figure 8C),  
524 highlighting the importance of KDM6B in coupling the two essential features of cancer cells. In summary,  
525 we have defined a novel chromatin-dependent mechanism of action of KDM6B inhibition that modulates  
526 the CDK4/6-pRB-E2F pathway in neuroblastoma. We also demonstrate that E2F target genes can act as  
527 biomarkers for sensitivity to KDM6B inhibitors in neuroblastoma and that this may well be predictive for  
528 other MYC-driven tumors.

529

530

## 531 **MATERIALS AND METHODS**

532

### 533 **Cell Culture and Reagents**

534 Neuroblastoma cell lines BE2(C) (ATCC), SIMA (DSMZ, Germany), SKNDZ (ATCC), SK-N-AS  
535 (ATCC), SK-N-SH (ATCC), IMR32 (ATCC), CHLA20 (COG), NB-1691 (Peter Houghton), HS68  
536 (ATCC) were cultured in standard RPMI media supplemented with 10% FBS (Sigma), 1% L-glutamine  
537 (MediaTech), at 37 °C in 5% CO<sub>2</sub>. Colorectal cancer cell lines HCT116, and isogenic p53<sup>-/-</sup> HCT116 cells  
538 were kindly provided by Bert Vogelstein (Baltimore, MD), osteosarcoma cell line U2OS, lung cancer cell  
539 lines A549 purchased from ATCC, and they were cultured in standard DMEM media supplemented with  
540 10% FCBS, 1% L-glutamine (MediaTech), at 37 °C in 5% CO<sub>2</sub>. Cell lines were validated by short tandem  
541 repeat (STR) using Promega PowerPlex 16 HS System once per month. PCR-based method was used for  
542 detection of Mycoplasma with LookOut Mycoplasma PCR Detection Kit (Sigma) and JumpStart Taq  
543 DNA Polymerase (Sigma) once per month to ensure cells were mycoplasma negative. GSK-J4,



544 Palbociclib, 17-DMAG, JQ-1 were purchased from Selleckchem. KDM5-C70 was purchased from Xcess  
545 Biosciences Inc.

#### 546 **AlphaLISA**

547 Materials: GSK J1 is purchased from Tocris (Bristol, United Kingdom, Catalog number 4593). 2,4-  
548 Pyridine Dicarboxylic Acid (2,4-PCA) is purchased from Acros Organics (New Jersey, Catalog number  
549 101860010). JIB-04 is purchased from Sigma-Aldrich (St. Louis, MO, Catalog number SML0808).  
550 Daminozide is purchased from Tocris (Bristol, United Kingdom, MO, Catalog number 4684). AlphaLISA  
551 anti-mIgG acceptor beads from PerkinElmer (Santa Clara, CA, Catalog number AL105C). AlphaLISA  
552 anti-rIgG acceptor beads from PerkinElmer (Santa Clara, CA, Catalog number AL104C). AlphaScreen  
553 Streptavidin-conjugated donor beads from PerkinElmer (Santa Clara, CA, Catalog number 6760002).  
554 Primary antibody 5 from BPS (Catalog number 52140E). Primary antibody 6 from BPS (Catalog number  
555 52140F). Primary antibody 13-4 from BPS (Catalog number 52140M4). Primary antibody 16-2 from BPS  
556 (Catalog number 52140P-2). Primary antibody 17-4 from BPS (Catalog number 52140Q4). Biotinylated  
557 histone H3 peptide substrate (KDM4A) BPS (Catalog number 79841). Biotinylated histone H3 peptide  
558 substrate (KDM5A) BPS (Catalog number 79840). Biotinylated histone H3 peptide substrate (KDM2A)  
559 BPS (Catalog number 79843). Biotinylated histone H3 peptide substrate (KDM6A and KDM6B) BPS  
560 (Catalog number 79841). Biotinylated histone H3 peptide substrate (KDM3A) BPS (Catalog number  
561 79841). 4x HDM Assay Buffer 2 from BPS (Catalog number 52407). 4x HDM Assay Buffer 3 from BPS  
562 (Catalog number 52408). 4x HDM Assay Buffer 4 from BPS (Catalog number 52409). 4x HDM Assay  
563 Buffer 5 from BPS (Catalog number 79847). 4x Detection buffer from BPS (Catalog number 52301).

564 Assay Conditions: All of the enzymatic reactions were conducted in duplicate at room temperature for 60  
565 minutes in a 10  $\mu$ l mixture containing assay buffer, histone H3 peptide substrate, demethylase enzyme,  
566 and the test compound. These 10  $\mu$ l reactions were carried out in wells of 384-well Optiplate  
567 (PerkinElmer). The dilution of the control compounds was first performed in 100 % DMSO. Each  
568 intermediate compound dilution (in 100 % DMSO) will then get directly diluted 30x fold into assay buffer  
569 for 3.3x conc (DMSO). Enzyme only and blank only wells have a final DMSO concentration of 1 %.  
570 From this intermediate step, 3  $\mu$ l of compound is added to 4  $\mu$ l of demethylase enzyme dilution is  
571 incubated for 30 minutes at room temperature. After this incubation, 3  $\mu$ l of peptide substrate is added.  
572 The final DMSO concentration is 1 %. After enzymatic reactions, 5  $\mu$ l of anti-Mouse Acceptor beads  
573 (PerkinElmer, diluted 1:500 with 1x detection buffer) or 5  $\mu$ l of anti-Rabbit Acceptor beads (PerkinElmer,  
574 diluted 1:500 with 1x detection buffer) and 5  $\mu$ l of Primary antibody (BPS, diluted 1:200 with 1x detection

575 buffer) were added to the reaction mix. After brief shaking, plate was incubated for 30 minutes. Finally,  
576 10  $\mu$ l of AlphaScreen Streptavidin-conjugated donor beads (Perkin, diluted 1:125 with 1x detection buffer)  
577 were added. In 30 minutes, the samples were measured in AlphaScreen microplate reader (EnSpire Alpha  
578 2390 Multilabel Reader, PerkinElmer).

579 Data Analysis: Enzyme activity assays were performed in duplicates at each concentration. The A-screen  
580 intensity data were analyzed and compared. In the absence of the compound, the intensity ( $C_e$ ) in each  
581 data set was defined as 100 % activity. In the absence of enzyme, the intensity ( $C_0$ ) in each data set was  
582 defined as 0 % activity. The percent activity in the presence of each compound was calculated according  
583 to the following equation: % activity =  $(C - C_0)/(C_e - C_0)$ , where C = the A-screen intensity in the presence  
584 of the compound. The values of % activity were plotted on a bar graph.

### 585 **SDS-PAGE and Western blotting**

586 For western blotting, samples were mixed with calculated volume of 2X sample buffer (1M TRIS/HCl,  
587 10% SDS, 0.1% bromophenol-blue, 10%  $\beta$ -mercaptoethanol, 10% glycerol), and heated for 25 minutes  
588 at 96°C. Proteins were resolved on SDS-polyacrylamide gels (SDS-PAGE) and transferred onto PVDF  
589 membrane (Immobilon-P, Millipore). After being incubated with the primary antibody, horseradish  
590 peroxidase-(HRP) conjugated secondary antibody (Novex, Life technologies) at 1: 5000 was used for 1  
591 hour incubation. The signals were detected by chemiluminescence (ECL, Thermo scientific). Antibodies  
592 including H3K4me1 (Abcam Cat# ab8895, RRID:AB\_306847), H3K4me3 (RevMAb Biosciences Cat#  
593 31-1226-00, RRID:AB\_2783580), H3K27ac (Active Motif Cat# 39133, RRID:AB\_2561016),  
594 H3K27me3 (Cell Signaling Technology Cat# 9733, RRID:AB\_2616029), CDK4 (Cell Signaling  
595 Technology Cat# 12790, RRID:AB\_2631166), CDK6 (Cell Signaling Technology Cat# 13331,  
596 RRID:AB\_2721897),  $\beta$ -ACTIN (Sigma-Aldrich Cat# A1978, RRID:AB\_476692), GAPDH (Cell  
597 Signaling Technology Cat# 5174, RRID:AB\_10622025), pRB (4H1) (Cell Signaling Technology Cat#  
598 9309, RRID:AB\_823629), MYCN (Cell Signaling Technology Cat# 9405, RRID:AB\_10692664) or  
599 (Santa Cruz Biotechnology Cat# sc-53993, RRID:AB\_831602), C-MYC (Cell Signaling Technology Cat#  
600 13987, RRID:AB\_2631168), KDM6B (Abclonal, A12763), H3K9me3 (Active Motif, 39161),  
601 H3K36me3 (Abcam, ab9050), were used for western blot.

602

### 603 **Crystal Violet Staining**

604 After removing media, cells were washed with Dulbecco's phosphate buffered saline without calcium or  
605 magnesium (DPBS, Lonza) and treated with 4% Formaldehyde in PBS (PFA) for 20 minutes. Once PFA  
606 was removed, cells were stained with 0.1% crystal violet stain for 1 hour.

607

### 608 **Synergy Assay**

609 BE2C and SK-N-AS cells were seeded in 96-well plates (3,000 cells per well). After 24 hours, cells were  
610 treated with GSK-J4 (0, 0.25, 0.5, 1  $\mu$ M, for BE2C, 0, 0.5, 1, 2.5  $\mu$ M for SK-N-AS) and palbociclib (0,  
611 0.25, 0.5, 1.0, 2.0, 4.0  $\mu$ M) or JQ1 (0, 0.0625, 0.125, 0.25, 0.5, 1.0  $\mu$ M) or 17-DMAG (0, 0.0625, 0.125,  
612 0.25, 0.5, 1.0  $\mu$ M) in a 4x6 matrix. Every combination treatment was performed in quadruplicate. Cells  
613 were treated for 5 days, and cell viability was determined using the Prestoblu assay (Invitrogen, A-  
614 13262). Cell viability for each treatment was normalized against the control group. A Bliss independence  
615 model was used to evaluate combination effects. Percentage over the Bliss score index was calculated  
616 with the equation  $(A+B)-AxB$ , in which A and B are the percentage of growth inhibitions induced by  
617 agents A and B at a given dose, respectively. The difference between the Bliss expectation and the  
618 observed growth inhibition induced by the combination of agent A and B at the same dose is the Bliss  
619 excess.

620

### 621 **Cell viability assay**

622 BE2C, and CDK4 or CDK6 overexpressing BE2C (BE2C-CDK4-OE, BE2C-CDK6-OE) cells were  
623 seeded in 96-well plates at 3,000 cells per well. After 24 hours, cells were treated with GSK-J4 (0, 0.02,  
624 0.04, 0.08, 0.16, 0.3125, 0.625, 1.25, 2.5, 5.0, 10  $\mu$ M) and palbociclib (0, 0.02, 0.04, 0.08, 0.16, 0.3125,  
625 0.625, 1.25, 2.5, 5.0, 10  $\mu$ M). Cells were treated for 5 days. Cell viability was determined using the  
626 Prestoblu assay (Invitrogen, A-13262). Cell viability for each treatment was normalized against no  
627 treatment well. EC50 was determined with GraphPad Prism equation  $Y=100/(1+10^{((\text{LogEC50}-X)*\text{HillSlope}))}$ , EC50 is the concentration that gives a 50% response. HillSlope represents the steepness  
628 of the curve.

629

### 631 **Small interfering RNA Transfection**

632 Small interfering RNAs (siRNA) were transfected into subconfluent cells using Lipofectamine RNAiMax  
633 (Invitrogen) according to manufacturer's instructions. Non-Targeting siRNA#1 (Dharmacon, D-001810-  
634 0105) used as siRNA control. The siRNA oligos for KDM6B have sequences as follows: KDM6B#1, 5-  
635 GGAAUGAGGUGAAGAACGU-3, KDM6B#2, 5-GGAGACCUCGUGUGGAUUA-3, KDM6B#31, 5-



636 GCAUCUAUCUGGAGAGCAA-3, KDM6B#33, 5-GGAAGAGGAACAGCAACA-3. KDM6B-  
637 3'UTR, 5-AGAAAGAACUAUGAGGAAAUU-3.

638

### 639 **CRISPR knockout of Rb1**

640 The Rb1 CRISPR plasmid with gRNA sequence 5-GCTCTGGGTCCTCCTCAGGA-3 (TLCV2-RB1,  
641 Addgene#87836) was purchased from Addgene. Plasmids were maxipreped by using NucleoBond Xtra  
642 EF kits (Takara Bio USA, 740424-50) according to manufacturer's protocol. Lentivirus was produced by  
643 transient transfection of PEI-pro DNA complex (6µg of TLCV2-RB1, 3 µg of 1-1r, 1 µg RTR, 1 µg of  
644 VSVg with 22 ul of PEI pro in 400 µl of DMEM medium) with 5 x 10<sup>6</sup> HEK293T cells in 10 ml complete  
645 medium (DMEM, 100 U/mL penicillin/streptomycin, 1 x L-glutamine and 10% FBS) in a 10 cm dish.  
646 Virus supernatant was collected every 8-12 hours for 3 days, which were passed through a 0.45 µm filter  
647 and concentrated by ultracentrifuge at 28,500 rpm for 1.5 hours at 4°C. The TLCV2-RB1 virus particles  
648 were added to BE2C cells with polybrene to final concentration of 8 µg/ml. Puromycin (2.5 µg/ml in  
649 complete medium) selection were performed in the next day after virus transduction. To generate Rb1  
650 knockout in BE2C, BE2C-Rb1 cells were treated with 1µM of doxycycline for 72 h, then sorted for green  
651 fluorescent protein (GFP) positive cells to enrich for RB1 knockout. The sorted cells were expanded  
652 without doxycycline in RPMI 1640 media (Corning, 10-040-CM) supplemented with 100 U/mL  
653 penicillin/streptomycin (Gibco, 15140122), and 10% FBS (Sigma-Aldrich, F2442).

654

### 655 **Generation of KDM6B, CDK4 and CDK6 overexpressing cell lines**

656 The CDK4 plasmid (pHAGE-CDK4, Addgene#116724) and CDK6 plasmid (pHAGE-CDK6,  
657 Addgene#116725) were purchased from Addgene. The plasmid maxiprep and lentiviral packaging were  
658 followed by the same protocol as described in Rb1 knockout. To overexpress CDK4 and CDK6 in BE2C  
659 cells, the pHAGE-CDK4 or pHAGE-CDK6 viral particles were transduced to BE2C cells and sorted for  
660 green fluorescent protein (GFP) positive ones. To overexpression KDM6B, MSCV-JMJD3  
661 (Addgene#21212) were packaged into retroviral particles, which were transduced into BE2C cells and  
662 selected with puromycin for stable expression.

663

### 664 **RNA-seq and microarray**

665 Total RNA was extracted from cells by using RNeasy Mini Kit (cat. # 74104) from QIAGEN. Paired-end  
666 sequencing was performed using the High-Seq platform with 100bp read length. Reads were aligned to  
667 the human GRCh37-lite using SJCRH's Strongarm pipeline. Counts per gene were obtained using htseq-

668 count version 0.6.1 with Gencode vM5 level 1 and 2 gene annotations. Counts were normalized with  
669 VOOM and analyzed with LIMMA within the R statistical environment. Significance was defined as  
670 having a false discovery rate (FDR) <0.05. VOOM normalized counts were analyzed with Gene Set  
671 Enrichment Analysis (GSEA)<sup>92</sup>. For Affymetrix microarray, after quality control with Agilent RNA  
672 analyzer, RNA was subjected to hybridization using an Affymetrix Clariom S human array. Differential  
673 gene expression was analyzed by t-test using the Differential Expression Analysis  
674 module at GenePattern server (<http://genepattern.broadinstitute.org/gp/pages/protocols/DiffExp.html>).

675

### 676 **Assay for Transposase-Accessible Chromatin using sequencing (ATAC-seq)**

677 Library preparations for ATAC-seq were based on the protocol with minor modifications<sup>47,93</sup>. Briefly,  
678 fresh cultured BE2C cells (100,000 per sample) with or without 2.5 $\mu$ M of GSK-J4 treatment were  
679 harvested and washed with 150 $\mu$ l cold Dulbecco's Phosphate-Buffered Saline (DPBS) containing protease  
680 inhibitor (PI). Nuclei were collected by centrifuging at 500g for 10 minutes at 4°C after cell pellets were  
681 resuspended in lysis buffer (10 mM Tris-Cl pH 7.4, 10 mM NaCl, and 3 mM MgCl<sub>2</sub> containing 0.1% NP-  
682 40 and PI). Nuclei were incubated with Tn5 transposon enzyme in transposase reaction mix buffer  
683 (Illumina) for 30 min at 37°C. DNAs were purified from transposition sample by using Min-Elute PCR  
684 purification kit (Qiagen, Valencia, CA) and measured by Qubit. Polymerase chain reaction (PCR) was  
685 performed to amplify with High-Fidelity 2X PCR Master Mix [72°C/5mins+ 98 °C /30 s +12 × (98 °C /10  
686 s + 63 °C /30 s + 72 °C /60 s) + 72 °C /5 min]. The libraries were purified using Min-Elute PCR  
687 purification kit (Qiagen, Valencia, CA). ATAC-seq libraries followed by pair-end sequencing on  
688 HiSeq4000 (Illumina) in the Hartwell Center at St Jude Children's Research Hospital.

689

### 690 **ATAC-seq data analysis**

691 2x100bp paired-end reads obtained from all samples were trimming for Nextera adapter by  
692 cutadapt(version 1.9, paired-end mode, default parameter with “ -m 25 -O 6 ”)<sup>94</sup> and aligned to human  
693 genome hg19(GRCh37-lite) by BWA (version 0.7.12-r1039, default parameter)<sup>95</sup> , duplicated reads were  
694 then marked with Picard(version 2.6.0-SNAPSHOT)<sup>96</sup> and only non-duplicated proper paired reads have  
695 been kept by samtools (parameter “ -q 1 -F 1804 ” version 1.2)<sup>97</sup>. After adjustment of Tn5 shift (reads were  
696 offset were offset by +4 bp for the sense strand and -5 bp for the antisense strand) we separated reads into  
697 nucleosome free, mononucleosome, dinucleosome, trinucleosome as described in Buenrostro et.al<sup>98</sup> by  
698 fragment size and generated bigwig files by using the center 80bp of fragments and scale to 20M  
699 nucleosome free reads. We observed reasonable nucleosome free peaks and pattern of mono-, di-, tri-

700 nucleosome on IGV (version 2.4.13)<sup>99</sup>. Next we merged each 2 replicates to enhance peak calling on  
701 nucleosome free reads by MACS2(version 2.1.1.20160309 default parameters with “--extsize 200 --  
702 nomodel ”)<sup>100</sup>, all cell types have more than 20M nucleosome free reads after merge so we consider all  
703 important nucleosome free regions were called. To assure the replicability, we first merge peaks from  
704 different treatmeans to create a set of reference chromatin accessible regions. We then counted  
705 nucleosome free reads from each of samples overlap the reference regions by bedtools (v2.24.0)<sup>101</sup>. We  
706 conclude the reproducibility is good since spearman correlation coefficient between replicates are larger  
707 than between samples from different groups. To find the differential accessible regions, we first  
708 normalized raw nucleosome free reads counts used trimmed mean of M-values normalization  
709 method(TMM) and applied Empirical Bayes Statistics test after linear fitting from voom package(R 3.23,  
710 edgeR 3.12.1, limma 3.26.9)<sup>102</sup>. FDR-correct p-value 0.05 and fold change > 2 were used as cutoff for  
711 differential accessible regions (DARs) while p-value > 0.5 and fold change < 1.05 were used for control  
712 regions. To find the Transcription factor enriched for DARs, we scanned the TRANSFAC <sup>103</sup> motif  
713 database using FIMO(parameter “--motif-pseudo 0.0001 --thresh 1e-4”) from MEME suite(v4.11.3)<sup>104</sup>,  
714 then for each motif, we counted how many DARs or control regions have the motif matches and using  
715 Fisher exact test to estimate their enrichment over the background(DAR or control regions don’t have the  
716 motif matches).

717

### 718 **CUT&Tag and analysis**

719 CUT&Tag for KDM6B knockdown and GSK-J4 treatment was prepared by following the protocol as  
720 described previously (Kaya-Okur et al. 2019 and [https://www.protocols.io/view/bench-top-cut-amp-tag-  
721 bcuhiwt6?step=1](https://www.protocols.io/view/bench-top-cut-amp-tag-bcuhiwt6?step=1) ) with minor modifications. Approximately 500,000 BE2C cells were treated with  
722 siRNAs (siCtrl or siKDM6B) or compounds (DMSO 0.1% or GSK-J4 2.5 $\mu$ M) for 72 hours, followed by  
723 washing with wash buffer (20 mM HEPES pH 7.5; 150 mM NaCl; 0.5 mM Spermidine; 1 $\times$  Protease  
724 inhibitor cocktail). Nuclei were isolated with cold NE1 buffer (20 mM HEPES–KOH, pH 7.9; 10 mM  
725 KCl 0.1%; Triton X-100; 20% Glycerol, 0.5 mM Spermidine; 1x Protease Inhibitor) for 10 min on ice.  
726 Nuclei were collected by 600 x g centrifuge and resuspended in 1ml washing buffer containing with 10  $\mu$ L  
727 of activated concanavalin A-coated beads (Bangs laboratories, BP531) at RT for 10 min. Bead-bound  
728 nuclei were collected with placing tube on magnet stand and removing clear liquid. The nuclei bound with  
729 bead were resuspended in 50  $\mu$ L Dig-150 buffer (20 mM HEPES pH 7.5; 150 mM NaCl; 0.5 mM  
730 Spermidine; 1 $\times$  Protease inhibitor cocktail; 0.05% Digitonin; 2 mM EDTA) and incubated with a 1:50  
731 dilution of H3K4me1 (Abcam, ab8895) and H3K27me3 (CST, 9733S) antibodies overnight at 4 °C. The

732 unbound primary antibody was removed by placing the tube on the magnet stand and withdrawing the  
733 liquid. The primary antibody bound nuclei bead was mixed with 100uL of Dig-150 buffer containing  
734 guinea pig anti-Rabbit IgG antibody (Antibodies, ABIN101961) in 1:100 dilution for 1 hour at RT. Beads  
735 bound nuclei were washed using the magnet stand 3× for 5 min in 1 mL Dig-150 buffer to remove unbound  
736 antibodies. A 1:100 dilution of pA-Tn5 adapter complex was prepared in Dig-300 buffer (20 mM HEPES,  
737 pH 7.5, 300 mM NaCl, 0.5 mM Spermidine, 0.05% Digitonin, 1× Protease inhibitor cocktail). After  
738 removing the liquid on the magnet stand, 100 μL mixture of pA-Tn5 and Dig- 300 buffer was added to  
739 the nuclei bound beads with gentle vortex and incubated at RT for 1 h. After 3× 5 min in 1 mL Dig-300  
740 buffer to remove unbound pA-Tn5 protein, nuclei were resuspended in 250 μL Tagmentation buffer  
741 (10 mM MgCl<sub>2</sub> in Dig-300 buffer) and incubated at 37 °C for 1 h. 10 μL of 0.5 M EDTA, 3 μL of 10%  
742 SDS and 2.5 μL of 20 mg/mL Proteinase K were added to stop tagmentation and incubated at 55 °C for 1  
743 hour. DNA was then precipitated by phenol/chloroform/isoamylalcohol followed by ethanol precipitation  
744 with glycogen and then dissolved in water. Sequencing libraries were prepared using NEBNext HiFi 2×  
745 PCR Master Mix (NEB, M0541L) according to the manufacturer's instructions. The PCR products were  
746 cleaned up with SPRIselect beads and quantified using Qubit dsDNA HS assay kit (Agilent Technologies).  
747 The libraries were sequenced on a HiSeq2500 with paired-end 50-bp reads (Illumina).  
748 Mapping reads and peak calling. The Cut&Tag raw reads were aligned to the human reference genome  
749 (hg19) using BWA (version 0.7.12; BWA aln+sampe). Duplicate reads were marked and removed by  
750 Picard (version 1.65). Only properly paired uniquely mapped reads with a fragment size of 150bp-2000bp  
751 were extracted by samtools (version 1.3.1 parameters used were -q 1 -f 2 -F 1804) for calling peaks and  
752 generating bigwig file. Narrow peaks were called by MACS2 (version 2.2.7.1) with parameters of “ -t  
753 cut\_tag\_file -q 0.05 -f BED --keep-dup all” for CUT&Tag data). We used SICER (version 1.1, with  
754 parameters of redundancy threshold 1, window size 200bp, effective genome fraction 0.86, gap size  
755 600bp, FDR 0.00001 with fragment size defined above) for calling broad enriched regions. Unmapped  
756 reads were further aligned to E.Coli genome as a spike-in control to calculate CHIP-Rx scaling factor as  
757 described<sup>105,106</sup>. The Cut&Tag library size of each sample was adjusted by E.Coli spike-in scaling factor  
758 and then used to normalize the read count for the downstream differential analysis, IGV bigwig and  
759 heatmap visualization.

760 Visualization. We used genomeCoverageBed (BEDtools 2.25.0) to produce genome-wide coverage in  
761 BEDGRAPH file and then converted it to a bigwig file by bedGraphToBigWig. The bigwig signals were  
762 adjusted by E.Coli spike-in scaling factor and scaled to 15 million reads to allow comparison across  
763 samples. To show average of several replicates as a single track in the browser, the bigwig files were

764 merged to a single average bigwig file using UCSC tools bigWigtoBedGraph, bigWigMerge and  
765 bedGraphToBigWig. The Integrated Genomics Viewer (IGV 2.3.82) was used for visual exploration of  
766 data. DeepTools (version 2.3)<sup>107</sup> was used to plot heatmap.

767 Differential analysis. Cut&Tag raw read counts were reported for each region/each sample using  
768 BEDtools 2.25.0. Raw read counts were Voom normalized and statistically contrasted using the R  
769 (version 3.5.1) packages limma and edgeR (version 3.16.5) for CPM calculation and differential analysis.  
770 An empirical Bayes fit was applied to contrast treated samples to control samples and to generate log fold  
771 changes, p values and false discovery rates for each peak region.

772 Peak overlap and annotation. Peak regions were defined to be the union of peak intervals in replicates  
773 from control or treated cells respectively. For peak overlap analysis, mergeBed (BEDtools version 2.25.0)  
774 was used to combine overlapping regions from multiple peak sets into a new region and then a custom  
775 script was used to summarize common or distinct peaks and visualize in a venn diagram. Promoter regions  
776 was defined as the regions 1.0 kb upstream and 1.0 kb downstream of the transcription start sites based  
777 on the human RefSeq annotation (hg19). Genomic feature annotation of peaks was done by  
778 annotatePeaks.pl, a program from the HOMER suite (v4.8.3, <http://homer.salk.edu/homer/>).

779 Motif analysis. Adjacent histone mark peaks (within a distance of 100bp) from both control and treated  
780 samples were merged first and then separated to 3 subgroups including control-only, treatment-only and  
781 shared peaks (at least 1bp overlap) using Bedtools (version 2.25.0). The regions of peak center +/- 100 bp  
782 were used for HOMER known motif search. Top ten most significant motifs from each sub-group were  
783 visualized as a heatmap.

784

### 785 **Hi-C data mining**

786 To view the 3D chromatin conformation of *MYCN* and *E2F8* gene in BE2C, we mined the Hi-C data, of  
787 BE2C, KELLY and SK-N-AS cells, which were downloaded from St Jude Cloud  
788 (<https://www.stjude.cloud/>)<sup>108</sup>. The Arc TRAC data showing the chromatin interactions, which were  
789 generated from Jurkat ChIA-PET SMC1 (Mango), were downloaded from St Jude Protein Paint program  
790 under St Jude Cloud (<https://proteinpaint.stjude.org/>).

791

### 792 **Library of Integrated Network-based Cellular Signatures (LINCS) analysis**

793 We had two sets of gene expression data: microarray and RNA-seq for siKDM6B and GSK-J4 treatment.  
794 While the pathway analysis showed very similar results for each, we used them in different purposes.  
795 Because Lincs used a limited number of genes in characterizing chemical compounds signatures, we chose

796 our microarray data to compare since RNA-seq data gave rise to a large amount of gene expression data  
797 that were not covered by Lincs chemical signatures. We first identify differentially expressed genes in  
798 microarray data using GenePattern program  
799 (<https://cloud.genepattern.org/gp/pages/index.jsf>). Then we chose the downregulated genes (with logFC  
800  $\geq 0.7$ ) by KDM6B knockdown or GSK-J4 treatment to compare with the chemical signatures in LINCS  
801 database (<http://www.lincsproject.org/LINCS/tools>). The datasets from LINCS L1000 Chem Pert down  
802 were downloaded and analyzed using PRISM program.

803

### 804 **The Cancer Therapeutics Response Portal (CTRP) analysis**

805 Cancer Therapeutic Response Portal (<https://portals.broadinstitute.org/ctrp.v2.1/>) correlated the  
806 sensitivity patterns of 481 compounds including GSK-J4 with 19,000 basal transcript levels across 823  
807 different human cancer cell lines and identified selective outlier transcripts<sup>44,45</sup>, which allowed to  
808 interrogate whether KDM6B inhibitor was correlated with specific transcripts. We chose the features that  
809 show the correlation of drug sensitivity with gene expression or copy number of queried genes such as  
810 E2F8.

811

### 812 **Kaplan-Meier analysis**

813 A 149-gene signature commonly downregulated by GSK-J4 in BE2C and three other neuroblastoma cell  
814 lines (IMR5, LAN5 and SK-N-FI)<sup>43</sup> was uploaded into R2 genomics analysis and visualization program  
815 (<https://hgserver1.amc.nl/cgi-bin/r2/main.cgi>) to find the differentially expressed genes in high-risk  
816 neuroblastoma in dataset (GSE49710) that has 498 cases, followed by k-means cluster analysis. The 4  
817 clusters were stored as track for Kaplan-Meier curve analysis using Log-Rank method for event-free  
818 survival and overall survival.

819

### 820 **Statistical analysis**

821 To determine statistical significance, the unpaired, two-tailed Student *t* test was calculated using the *t* test  
822 calculator available on GraphPad Prism 8.0 software. A *p* value of less than 0.05 was considered  
823 statistically significant.

824

### 825 **Data accessibility**

826 Super series GSE149539 includes 3 datasets.

827 <https://www.ncbi.nlm.nih.gov/geo/query/acc.cgi?acc=GSE149539&token=ehozmooupbajlaf>



828 GSE182884 [CUT&TAG]  
829 KDM6B regulates an CDK4/6-pRB-E2F transcriptome that is correlated with GSK-J4 sensitivity  
830 GSE149519 [ATAC-seq]  
831 KDM6B regulates an CDK4/6-pRB-E2F transcriptome that is correlated with GSK-J4 sensitivity  
832 GSE149537 [RNA-seq]  
833 KDM6B regulates an CDK4/6-pRB-E2F transcriptome that is correlated with GSK-J4 sensitivity  
834

### 835 **Acknowledgments**

836 This work was partly supported by American Cancer Society-Research Scholar (130421-RSG-17-071-01-  
837 TBG, Jun Yang) and National Cancer Institute (1R01CA229739-01, Jun Yang). The content is solely the  
838 responsibility of the authors and does not necessarily represent the official views of the National Institutes  
839 of Health.

840

### 841 **Contributions**

842 Alexandra D'Oto, Jie Fang, Shivendra Singh, Anoushka Mullasseril, Victoria Jones, Xinyu von Buttlar,  
843 Bailey Cooke, Dongli Hu, Ahmed Abu-Zaid performed experiments. Beisi Xu and Hongjian Jin analyzed  
844 sequencing data. Jun Yang and Andrew M Davidoff conceived the project. Jun Yang wrote the  
845 manuscript with input from Jason Shohet, Andrew J Murphy and Andrew M Davidoff.

### 846 **References**

847

- 848 1 Agger, K. *et al.* UTX and JMJD3 are histone H3K27 demethylases involved in  
849 HOX gene regulation and development. *Nature* **449**, 731-734,  
850 doi:10.1038/nature06145 (2007).
- 851 2 De Santa, F. *et al.* The histone H3 lysine-27 demethylase Jmjd3 links  
852 inflammation to inhibition of polycomb-mediated gene silencing. *Cell* **130**,  
853 1083-1094, doi:10.1016/j.cell.2007.08.019 (2007).
- 854 3 Hong, S. *et al.* Identification of JmjdC domain-containing UTX and JMJD3 as  
855 histone H3 lysine 27 demethylases. *Proc Natl Acad Sci U S A* **104**, 18439-  
856 18444, doi:10.1073/pnas.0707292104 (2007).
- 857 4 Xiang, Y. *et al.* JMJD3 is a histone H3K27 demethylase. *Cell Res* **17**, 850-857,  
858 doi:10.1038/cr.2007.83 (2007).
- 859 5 Margueron, R. *et al.* Ezh1 and Ezh2 maintain repressive chromatin through  
860 different mechanisms. *Mol Cell* **32**, 503-518,  
861 doi:10.1016/j.molcel.2008.11.004 (2008).
- 862 6 Walport, L. J. *et al.* Human UTY(KDM6C) is a male-specific N-methyl lysyl  
863 demethylase. *J Biol Chem* **289**, 18302-18313, doi:10.1074/jbc.M114.555052  
864 (2014).

- 865 7 Kandoth, C. *et al.* Mutational landscape and significance across 12 major  
866 cancer types. *Nature* **502**, 333-339, doi:10.1038/nature12634 (2013).
- 867 8 Huether, R. *et al.* The landscape of somatic mutations in epigenetic regulators  
868 across 1,000 paediatric cancer genomes. *Nat Commun* **5**, 3630,  
869 doi:10.1038/ncomms4630 (2014).
- 870 9 Agger, K. *et al.* The H3K27me3 demethylase JMJD3 contributes to the  
871 activation of the INK4A-ARF locus in response to oncogene- and stress-  
872 induced senescence. *Genes Dev* **23**, 1171-1176, doi:10.1101/gad.510809  
873 (2009).
- 874 10 Barradas, M. *et al.* Histone demethylase JMJD3 contributes to epigenetic  
875 control of INK4a/ARF by oncogenic RAS. *Genes Dev* **23**, 1177-1182,  
876 doi:10.1101/gad.511109 (2009).
- 877 11 Ene, C. I. *et al.* Histone demethylase Jumonji D3 (JMJD3) as a tumor  
878 suppressor by regulating p53 protein nuclear stabilization. *PLoS One* **7**,  
879 e51407, doi:10.1371/journal.pone.0051407 (2012).
- 880 12 Yamamoto, K. *et al.* Loss of histone demethylase KDM6B enhances  
881 aggressiveness of pancreatic cancer through downregulation of C/EBPalpha.  
882 *Carcinogenesis* **35**, 2404-2414, doi:10.1093/carcin/bgu136 (2014).
- 883 13 Arcipowski, K. M., Martinez, C. A. & Ntziachristos, P. Histone demethylases in  
884 physiology and cancer: a tale of two enzymes, JMJD3 and UTX. *Curr Opin*  
885 *Genet Dev* **36**, 59-67, doi:10.1016/j.gde.2016.03.010 (2016).
- 886 14 Ntziachristos, P. *et al.* Contrasting roles of histone 3 lysine 27 demethylases  
887 in acute lymphoblastic leukaemia. *Nature* **514**, 513-517,  
888 doi:10.1038/nature13605 (2014).
- 889 15 Ohguchi, H. *et al.* KDM6B modulates MAPK pathway mediating multiple  
890 myeloma cell growth and survival. *Leukemia*, doi:10.1038/leu.2017.141  
891 (2017).
- 892 16 Sherry-Lynes, M. M., Sengupta, S., Kulkarni, S. & Cochran, B. H. Regulation of  
893 the JMJD3 (KDM6B) histone demethylase in glioblastoma stem cells by  
894 STAT3. *PLoS One* **12**, e0174775, doi:10.1371/journal.pone.0174775 (2017).
- 895 17 Tang, B. *et al.* Aberrant JMJD3 Expression Upregulates Slug to Promote  
896 Migration, Invasion, and Stem Cell-Like Behaviors in Hepatocellular  
897 Carcinoma. *Cancer Res* **76**, 6520-6532, doi:10.1158/0008-5472.CAN-15-  
898 3029 (2016).
- 899 18 Dalvi, M. P. *et al.* Taxane-Platin-Resistant Lung Cancers Co-develop  
900 Hypersensitivity to JumonjiC Demethylase Inhibitors. *Cell Rep* **19**, 1669-  
901 1684, doi:10.1016/j.celrep.2017.04.077 (2017).
- 902 19 Maris, J. M. Recent advances in neuroblastoma. *N Engl J Med* **362**, 2202-2211,  
903 doi:10.1056/NEJMra0804577 (2010).
- 904 20 Cheung, N. K. & Dyer, M. A. Neuroblastoma: developmental biology, cancer  
905 genomics and immunotherapy. *Nat Rev Cancer* **13**, 397-411,  
906 doi:10.1038/nrc3526 (2013).
- 907 21 Bosse, K. R. & Maris, J. M. Advances in the translational genomics of  
908 neuroblastoma: From improving risk stratification and revealing novel  
909 biology to identifying actionable genomic alterations. *Cancer*,  
910 doi:10.1002/cncr.29706 (2015).



- 911 22 Gustafson, W. C. & Weiss, W. A. Myc proteins as therapeutic targets. *Oncogene*  
912 **29**, 1249-1259, doi:10.1038/onc.2009.512 (2010).
- 913 23 Chipumuro, E. *et al.* CDK7 inhibition suppresses super-enhancer-linked  
914 oncogenic transcription in MYCN-driven cancer. *Cell* **159**, 1126-1139,  
915 doi:10.1016/j.cell.2014.10.024 (2014).
- 916 24 Puissant, A. *et al.* Targeting MYCN in neuroblastoma by BET bromodomain  
917 inhibition. *Cancer Discov* **3**, 308-323, doi:10.1158/2159-8290.CD-12-0418  
918 (2013).
- 919 25 He, S., Liu, Z., Oh, D. Y. & Thiele, C. J. MYCN and the epigenome. *Front Oncol* **3**,  
920 1, doi:10.3389/fonc.2013.00001 (2013).
- 921 26 Yang, J. *et al.* The role of histone demethylase KDM4B in Myc signaling in  
922 neuroblastoma. *J Natl Cancer Inst* **107**, djv080, doi:10.1093/jnci/djv080  
923 (2015).
- 924 27 Yang, J. *et al.* Targeting Histone Demethylases in MYC-Driven  
925 Neuroblastomas with Ciclopirox. *Cancer Res* **77**, 4626-4638,  
926 doi:10.1158/0008-5472.CAN-16-0826 (2017).
- 927 28 Chen, L. *et al.* CRISPR-Cas9 screen reveals a MYCN-amplified neuroblastoma  
928 dependency on EZH2. *J Clin Invest* **128**, 446-462, doi:10.1172/JCI90793  
929 (2018).
- 930 29 Matthay, K. K. *et al.* Neuroblastoma. *Nat Rev Dis Primers* **2**, 16078,  
931 doi:10.1038/nrdp.2016.78 (2016).
- 932 30 Molenaar, J. J. *et al.* Sequencing of neuroblastoma identifies chromothripsis  
933 and defects in neuritogenesis genes. *Nature* **483**, 589-593,  
934 doi:10.1038/nature10910 (2012).
- 935 31 Fix, A. *et al.* Characterization of amplicons in neuroblastoma: high-resolution  
936 mapping using DNA microarrays, relationship with outcome, and  
937 identification of overexpressed genes. *Genes Chromosomes Cancer* **47**, 819-  
938 834, doi:10.1002/gcc.20583 (2008).
- 939 32 Lastowska, M. *et al.* Identification of candidate genes involved in  
940 neuroblastoma progression by combining genomic and expression  
941 microarrays with survival data. *Oncogene* **26**, 7432-7444,  
942 doi:10.1038/sj.onc.1210552 (2007).
- 943 33 Bannister, A. J. & Kouzarides, T. Regulation of chromatin by histone  
944 modifications. *Cell Res* **21**, 381-395, doi:10.1038/cr.2011.22 (2011).
- 945 34 Whyte, W. A. *et al.* Master transcription factors and mediator establish super-  
946 enhancers at key cell identity genes. *Cell* **153**, 307-319,  
947 doi:10.1016/j.cell.2013.03.035 (2013).
- 948 35 Pott, S. & Lieb, J. D. What are super-enhancers? *Nat Genet* **47**, 8-12,  
949 doi:10.1038/ng.3167 (2015).
- 950 36 Dyson, N. J. RB1: a prototype tumor suppressor and an enigma. *Genes Dev* **30**,  
951 1492-1502, doi:10.1101/gad.282145.116 (2016).
- 952 37 Thurlings, I. & de Bruin, A. E2F Transcription Factors Control the Roller  
953 Coaster Ride of Cell Cycle Gene Expression. *Methods Mol Biol* **1342**, 71-88,  
954 doi:10.1007/978-1-4939-2957-3\_4 (2016).
- 955 38 Strieder, V. & Lutz, W. E2F proteins regulate MYCN expression in  
956 neuroblastomas. *J Biol Chem* **278**, 2983-2989, doi:10.1074/jbc.M207596200  
957 (2003).

- 958 39 Ishida, S., Shudo, K., Takada, S. & Koike, K. A direct role of transcription factor  
959 E2F in c-myc gene expression during granulocytic and macrophage-like  
960 differentiation of HL60 cells. *Cell Growth Differ* **6**, 229-237 (1995).
- 961 40 Kruidenier, L. *et al.* A selective jumonji H3K27 demethylase inhibitor  
962 modulates the proinflammatory macrophage response. *Nature* **488**, 404-408,  
963 doi:10.1038/nature11262 (2012).
- 964 41 Heinemann, B. *et al.* Inhibition of demethylases by GSK-J1/J4. *Nature* **514**,  
965 E1-2, doi:10.1038/nature13688 (2014).
- 966 42 Johansson, C. *et al.* Structural analysis of human KDM5B guides histone  
967 demethylase inhibitor development. *Nat Chem Biol* **12**, 539-545,  
968 doi:10.1038/nchembio.2087 (2016).
- 969 43 Lochmann, T. L. *et al.* Targeted inhibition of histone H3K27 demethylation is  
970 effective in high-risk neuroblastoma. *Sci Transl Med* **10**,  
971 doi:10.1126/scitranslmed.aao4680 (2018).
- 972 44 Rees, M. G. *et al.* Correlating chemical sensitivity and basal gene expression  
973 reveals mechanism of action. *Nat Chem Biol* **12**, 109-116,  
974 doi:10.1038/nchembio.1986 (2016).
- 975 45 Seashore-Ludlow, B. *et al.* Harnessing Connectivity in a Large-Scale Small-  
976 Molecule Sensitivity Dataset. *Cancer Discov* **5**, 1210-1223, doi:10.1158/2159-  
977 8290.CD-15-0235 (2015).
- 978 46 Bertoli, C., Skotheim, J. M. & de Bruin, R. A. Control of cell cycle transcription  
979 during G1 and S phases. *Nat Rev Mol Cell Biol* **14**, 518-528,  
980 doi:10.1038/nrm3629 (2013).
- 981 47 Buenrostro, J. D., Wu, B., Chang, H. Y. & Greenleaf, W. J. ATAC-seq: A Method  
982 for Assaying Chromatin Accessibility Genome-Wide. *Curr Protoc Mol Biol*  
983 **109**, 21 29 21-21 29 29, doi:10.1002/0471142727.mb2129s109 (2015).
- 984 48 Hoxhaj, G. & Manning, B. D. The PI3K-AKT network at the interface of  
985 oncogenic signalling and cancer metabolism. *Nat Rev Cancer* **20**, 74-88,  
986 doi:10.1038/s41568-019-0216-7 (2020).
- 987 49 Chaussepied, M. & Ginsberg, D. Transcriptional regulation of AKT activation  
988 by E2F. *Mol Cell* **16**, 831-837, doi:10.1016/j.molcel.2004.11.003 (2004).
- 989 50 Kaya-Okur, H. S., Janssens, D. H., Henikoff, J. G., Ahmad, K. & Henikoff, S.  
990 Efficient low-cost chromatin profiling with CUT&Tag. *Nat Protoc* **15**, 3264-  
991 3283, doi:10.1038/s41596-020-0373-x (2020).
- 992 51 Helmsauer, K. *et al.* Enhancer hijacking determines extrachromosomal  
993 circular MYCN amplicon architecture in neuroblastoma. *Nat Commun* **11**,  
994 5823, doi:10.1038/s41467-020-19452-y (2020).
- 995 52 Phillips, J. E. & Corces, V. G. CTCF: master weaver of the genome. *Cell* **137**,  
996 1194-1211, doi:10.1016/j.cell.2009.06.001 (2009).
- 997 53 Wendt, K. S. *et al.* Cohesin mediates transcriptional insulation by CCCTC-  
998 binding factor. *Nature* **451**, 796-801, doi:10.1038/nature06634 (2008).
- 999 54 Debruyne, D. N. *et al.* BORIS promotes chromatin regulatory interactions in  
1000 treatment-resistant cancer cells. *Nature* **572**, 676-680, doi:10.1038/s41586-  
1001 019-1472-0 (2019).
- 1002 55 Local, A. *et al.* Identification of H3K4me1-associated proteins at mammalian  
1003 enhancers. *Nat Genet* **50**, 73-82, doi:10.1038/s41588-017-0015-6 (2018).

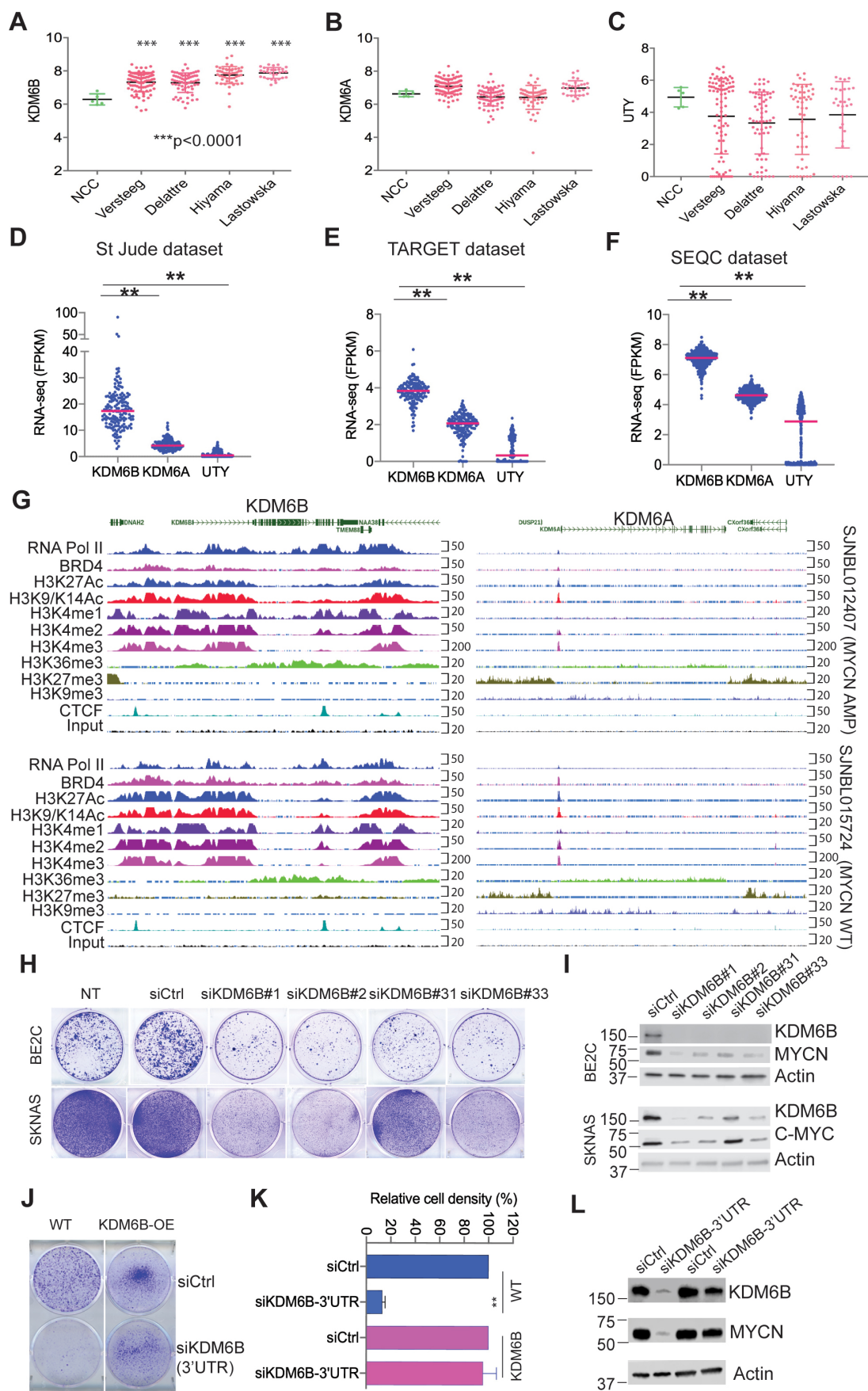
- 1004 56 Kagey, M. H. *et al.* Mediator and cohesin connect gene expression and  
1005 chromatin architecture. *Nature* **467**, 430-435, doi:10.1038/nature09380  
1006 (2010).
- 1007 57 Kim, S. I., Bultman, S. J., Kiefer, C. M., Dean, A. & Bresnick, E. H. BRG1  
1008 requirement for long-range interaction of a locus control region with a  
1009 downstream promoter. *Proc Natl Acad Sci U S A* **106**, 2259-2264,  
1010 doi:10.1073/pnas.0806420106 (2009).
- 1011 58 Beagrie, R. A. *et al.* Complex multi-enhancer contacts captured by genome  
1012 architecture mapping. *Nature* **543**, 519-524, doi:10.1038/nature21411  
1013 (2017).
- 1014 59 Rao, S. S. *et al.* A 3D map of the human genome at kilobase resolution reveals  
1015 principles of chromatin looping. *Cell* **159**, 1665-1680,  
1016 doi:10.1016/j.cell.2014.11.021 (2014).
- 1017 60 Bracken, A. P. *et al.* EZH2 is downstream of the pRB-E2F pathway, essential  
1018 for proliferation and amplified in cancer. *EMBO J* **22**, 5323-5335,  
1019 doi:10.1093/emboj/cdg542 (2003).
- 1020 61 Lee, S. R. *et al.* Activation of EZH2 and SUZ12 Regulated by E2F1 Predicts the  
1021 Disease Progression and Aggressive Characteristics of Bladder Cancer. *Clin*  
1022 *Cancer Res* **21**, 5391-5403, doi:10.1158/1078-0432.CCR-14-2680 (2015).
- 1023 62 Keenan, A. B. *et al.* The Library of Integrated Network-Based Cellular  
1024 Signatures NIH Program: System-Level Cataloging of Human Cells Response  
1025 to Perturbations. *Cell Syst* **6**, 13-24, doi:10.1016/j.cels.2017.11.001 (2018).
- 1026 63 Filippakopoulos, P. *et al.* Selective inhibition of BET bromodomains. *Nature*  
1027 **468**, 1067-1073, doi:10.1038/nature09504 (2010).
- 1028 64 Sherr, C. J., Beach, D. & Shapiro, G. I. Targeting CDK4 and CDK6: From  
1029 Discovery to Therapy. *Cancer Discov* **6**, 353-367, doi:10.1158/2159-8290.CD-  
1030 15-0894 (2016).
- 1031 65 Alvarez-Fernandez, M. & Malumbres, M. Mechanisms of Sensitivity and  
1032 Resistance to CDK4/6 Inhibition. *Cancer Cell* **37**, 514-529,  
1033 doi:10.1016/j.ccell.2020.03.010 (2020).
- 1034 66 Klein, M. E., Kovatcheva, M., Davis, L. E., Tap, W. D. & Koff, A. CDK4/6  
1035 Inhibitors: The Mechanism of Action May Not Be as Simple as Once Thought.  
1036 *Cancer Cell* **34**, 9-20, doi:10.1016/j.ccell.2018.03.023 (2018).
- 1037 67 Yang, L. *et al.* Histone demethylase KDM6B has an anti-tumorigenic function  
1038 in neuroblastoma by promoting differentiation. *Oncogenesis* **8**, 3,  
1039 doi:10.1038/s41389-018-0112-0 (2019).
- 1040 68 Hashizume, R. *et al.* Pharmacologic inhibition of histone demethylation as a  
1041 therapy for pediatric brainstem glioma. *Nat Med* **20**, 1394-1396,  
1042 doi:10.1038/nm.3716 (2014).
- 1043 69 Morozov, V. M., Li, Y., Clowers, M. M. & Ishov, A. M. Inhibitor of H3K27  
1044 demethylase JMJD3/UTX GSK-J4 is a potential therapeutic option for  
1045 castration resistant prostate cancer. *Oncotarget* **8**, 62131-62142,  
1046 doi:10.18632/oncotarget.19100 (2017).
- 1047 70 Mathur, R. *et al.* Inhibition of demethylase KDM6B sensitizes diffuse large B-  
1048 cell lymphoma to chemotherapeutic drugs. *Haematologica* **102**, 373-380,  
1049 doi:10.3324/haematol.2016.144964 (2017).

- 1050 71 Hong, B. J. *et al.* Oncogenic KRAS Sensitizes Lung Adenocarcinoma to GSK-J4-  
1051 Induced Metabolic and Oxidative Stress. *Cancer Res* **79**, 5849-5859,  
1052 doi:10.1158/0008-5472.CAN-18-3511 (2019).
- 1053 72 Hnisz, D. *et al.* Super-enhancers in the control of cell identity and disease. *Cell*  
1054 **155**, 934-947, doi:10.1016/j.cell.2013.09.053 (2013).
- 1055 73 Leone, G. *et al.* Myc requires distinct E2F activities to induce S phase and  
1056 apoptosis. *Mol Cell* **8**, 105-113, doi:10.1016/s1097-2765(01)00275-1 (2001).
- 1057 74 Chen, X. *et al.* Integration of external signaling pathways with the core  
1058 transcriptional network in embryonic stem cells. *Cell* **133**, 1106-1117,  
1059 doi:10.1016/j.cell.2008.04.043 (2008).
- 1060 75 Sherr, C. J. & McCormick, F. The RB and p53 pathways in cancer. *Cancer Cell* **2**,  
1061 103-112, doi:10.1016/s1535-6108(02)00102-2 (2002).
- 1062 76 Dick, F. A., Goodrich, D. W., Sage, J. & Dyson, N. J. Non-canonical functions of  
1063 the RB protein in cancer. *Nat Rev Cancer* **18**, 442-451, doi:10.1038/s41568-  
1064 018-0008-5 (2018).
- 1065 77 Easton, J., Wei, T., Lahti, J. M. & Kidd, V. J. Disruption of the cyclin D/cyclin-  
1066 dependent kinase/INK4/retinoblastoma protein regulatory pathway in  
1067 human neuroblastoma. *Cancer Res* **58**, 2624-2632 (1998).
- 1068 78 Krasnoselsky, A. L. *et al.* Altered expression of cell cycle genes distinguishes  
1069 aggressive neuroblastoma. *Oncogene* **24**, 1533-1541,  
1070 doi:10.1038/sj.onc.1208341 (2005).
- 1071 79 Molenaar, J. J. *et al.* Copy number defects of G1-cell cycle genes in  
1072 neuroblastoma are frequent and correlate with high expression of E2F target  
1073 genes and a poor prognosis. *Genes Chromosomes Cancer* **51**, 10-19,  
1074 doi:10.1002/gcc.20926 (2012).
- 1075 80 Mosse, Y. P. *et al.* Neuroblastomas have distinct genomic DNA profiles that  
1076 predict clinical phenotype and regional gene expression. *Genes Chromosomes*  
1077 *Cancer* **46**, 936-949, doi:10.1002/gcc.20477 (2007).
- 1078 81 Mosse, Y. P. *et al.* High-resolution detection and mapping of genomic DNA  
1079 alterations in neuroblastoma. *Genes Chromosomes Cancer* **43**, 390-403,  
1080 doi:10.1002/gcc.20198 (2005).
- 1081 82 Molenaar, J. J. *et al.* Cyclin D1 and CDK4 activity contribute to the  
1082 undifferentiated phenotype in neuroblastoma. *Cancer Res* **68**, 2599-2609,  
1083 doi:10.1158/0008-5472.CAN-07-5032 (2008).
- 1084 83 Rader, J. *et al.* Dual CDK4/CDK6 inhibition induces cell-cycle arrest and  
1085 senescence in neuroblastoma. *Clin Cancer Res* **19**, 6173-6182,  
1086 doi:10.1158/1078-0432.CCR-13-1675 (2013).
- 1087 84 Lee, M. G. *et al.* Demethylation of H3K27 regulates polycomb recruitment and  
1088 H2A ubiquitination. *Science* **318**, 447-450, doi:10.1126/science.1149042  
1089 (2007).
- 1090 85 Kim, J. H. *et al.* UTX and MLL4 coordinately regulate transcriptional programs  
1091 for cell proliferation and invasiveness in breast cancer cells. *Cancer Res* **74**,  
1092 1705-1717, doi:10.1158/0008-5472.CAN-13-1896 (2014).
- 1093 86 Wong, A. S. *et al.* Multiplexed barcoded CRISPR-Cas9 screening enabled by  
1094 CombiGEM. *Proc Natl Acad Sci U S A* **113**, 2544-2549,  
1095 doi:10.1073/pnas.1517883113 (2016).



- 1096 87 Yan, J. *et al.* Histone H3 lysine 4 monomethylation modulates long-range  
1097 chromatin interactions at enhancers. *Cell Res* **28**, 204-220,  
1098 doi:10.1038/cr.2018.1 (2018).
- 1099 88 Vernimmen, D. *et al.* Polycomb eviction as a new distant enhancer function.  
1100 *Genes Dev* **25**, 1583-1588, doi:10.1101/gad.16985411 (2011).
- 1101 89 Kartikasari, A. E. *et al.* The histone demethylase Jmjd3 sequentially associates  
1102 with the transcription factors Tbx3 and Eomes to drive endoderm  
1103 differentiation. *EMBO J* **32**, 1393-1408, doi:10.1038/emboj.2013.78 (2013).
- 1104 90 Fueyo, R. *et al.* Lineage specific transcription factors and epigenetic  
1105 regulators mediate TGFbeta-dependent enhancer activation. *Nucleic Acids*  
1106 *Res* **46**, 3351-3365, doi:10.1093/nar/gky093 (2018).
- 1107 91 Li, Z. *et al.* EZH2 regulates neuroblastoma cell differentiation via NTRK1  
1108 promoter epigenetic modifications. *Oncogene* **37**, 2714-2727,  
1109 doi:10.1038/s41388-018-0133-3 (2018).
- 1110 92 Subramanian, A. *et al.* Gene set enrichment analysis: a knowledge-based  
1111 approach for interpreting genome-wide expression profiles. *Proc Natl Acad*  
1112 *Sci U S A* **102**, 15545-15550, doi:10.1073/pnas.0506580102 (2005).
- 1113 93 Buenrostro, J. D., Giresi, P. G., Zaba, L. C., Chang, H. Y. & Greenleaf, W. J.  
1114 Transposition of native chromatin for fast and sensitive epigenomic profiling  
1115 of open chromatin, DNA-binding proteins and nucleosome position. *Nat*  
1116 *Methods* **10**, 1213-1218, doi:10.1038/nmeth.2688 (2013).
- 1117 94 Martin, M. Cutadapt removes adapter sequences from high-throughput  
1118 sequencing reads. *EMBnet.journal* **17**, pp.-10-12 (2011).
- 1119 95 Li, H. & Durbin, R. Fast and accurate short read alignment with Burrows-  
1120 Wheeler transform. *Bioinformatics* **25**, 1754-1760,  
1121 doi:10.1093/bioinformatics/btp324 (2009).
- 1122 96 Tischler, G. & Leonard, S. biobambam: tools for read pair collation based  
1123 algorithms on BAM files. *Source Code for Biology and Medicine* **9**, 13,  
1124 doi:10.1186/1751-0473-9-13 (2014).
- 1125 97 Li, H. *et al.* The Sequence Alignment/Map format and SAMtools.  
1126 *Bioinformatics* **25**, 2078-2079, doi:10.1093/bioinformatics/btp352 (2009).
- 1127 98 Buenrostro, J. D., Giresi, P. G., Zaba, L. C., Chang, H. Y. & Greenleaf, W. J.  
1128 Transposition of native chromatin for fast and sensitive epigenomic profiling  
1129 of open chromatin, DNA-binding proteins and nucleosome position. *Nature*  
1130 *Methods* **10**, 1213-1218, doi:10.1038/nmeth.2688 (2013).
- 1131 99 Robinson, J. T. *et al.* Integrative genomics viewer. *Nature Biotechnology* **29**,  
1132 24-26, doi:10.1038/nbt.1754 (2011).
- 1133 100 Zhang, Y. *et al.* Model-based Analysis of ChIP-Seq (MACS). *Genome Biology* **9**,  
1134 R137, doi:10.1186/gb-2008-9-9-r137 (2008).
- 1135 101 Quinlan, A. R. & Hall, I. M. BEDTools: a flexible suite of utilities for comparing  
1136 genomic features. *Bioinformatics* **26**, 841-842,  
1137 doi:10.1093/bioinformatics/btq033 (2010).
- 1138 102 Law, C. W., Chen, Y., Shi, W. & Smyth, G. K. voom: precision weights unlock  
1139 linear model analysis tools for RNA-seq read counts. *Genome Biology* **15**, R29,  
1140 doi:10.1186/gb-2014-15-2-r29 (2014).
- 1141 103 Matys, V. *et al.* TRANSFAC and its module TRANSCompel: transcriptional  
1142 gene regulation in eukaryotes. *Nucleic Acids Res* **34**, D108 - 110 (2006).

- 1143 104 Bailey, T. L. *et al.* MEME SUITE: tools for motif discovery and searching.  
1144 *Nucleic Acids Res* **37**, W202-208, doi:10.1093/nar/gkp335 (2009).
- 1145 105 Skene, P. J. & Henikoff, S. An efficient targeted nuclease strategy for high-  
1146 resolution mapping of DNA binding sites. *Elife* **6**, doi:10.7554/eLife.21856  
1147 (2017).
- 1148 106 Orlando, D. A. *et al.* Quantitative ChIP-Seq normalization reveals global  
1149 modulation of the epigenome. *Cell Rep* **9**, 1163-1170,  
1150 doi:10.1016/j.celrep.2014.10.018 (2014).
- 1151 107 Ramirez, F. *et al.* deepTools2: a next generation web server for deep-  
1152 sequencing data analysis. *Nucleic Acids Res* **44**, W160-165,  
1153 doi:10.1093/nar/gkw257 (2016).
- 1154 108 McLeod, C. *et al.* St. Jude Cloud: A Pediatric Cancer Genomic Data-Sharing  
1155 Ecosystem. *Cancer Discov* **11**, 1082-1099, doi:10.1158/2159-8290.CD-20-  
1156 1230 (2021).
- 1157 109 Zeid, R. *et al.* Enhancer invasion shapes MYCN-dependent transcriptional  
1158 amplification in neuroblastoma. *Nat Genet* **50**, 515-523,  
1159 doi:10.1038/s41588-018-0044-9 (2018).
- 1160
- 1161



1162 **Figure 1. KDM6B is marked with a highly active epigenetic landscape and highly expressed in**  
1163 **neuroblastoma and regulates MYC expression.**

1164 **(A-C)** The expression of KDM6B, KDM6A and UTY in normal human trunk neural crest (GSE14340)  
1165 and 4 different neuroblastoma cohorts (Versteeg GSE16476, Delattre GSE14880, Hiyama GSE16237,  
1166 Lastowska GSE13136). Y-axis represents the normalized log<sub>2</sub> expression value. \*\*\*p<0.001, student t  
1167 test

1168 **(D-F)** The expression of KDM6B, KDM6A and UTY in 3 different neuroblastoma RNA-seq cohorts. The  
1169 RNA-seq data of St Jude was downloaded from <https://pecan.stjude.cloud>. The RNA-seq data of  
1170 TARGET and SEQC datasets were downloaded from R2 (<https://hgserver1.amc.nl/cgi-bin/r2/main.cgi>).  
1171 Y-axis represents the Fragment Per Kilobase of transcript per Million (FPKM) mapped reads.

1172 **(G)** The epigenetic landscapes consisting of histone marks and transcription factor binding distinguish  
1173 KDM6B from KDM6A in primary neuroblastoma tissues with MYCN amplification or without MYCN  
1174 amplification ([https://pecan.stjude.cloud/proteinpaint/study/mycn\\_nbl\\_2018](https://pecan.stjude.cloud/proteinpaint/study/mycn_nbl_2018)).

1175 **(H)** Crystal violet staining of colonies after BE2C and SKNAS cells were transfected with four different  
1176 siRNA oligos to knockdown KDM6B for 7 days. siCtrl = siRNA control oligo, NT= no treatment.

1177 **(I)** Western blot analysis with indicated antibodies to assess MYCN or C-MYC expression after 3-day  
1178 transfection of 4 different siRNA to knockdown KDM6B in BE2C and SKNAS.

1179 **(J)** BE2C and MSCV-KDM6B overexpressing (KDM6B-OE) BE2C cells were transfected with siRNA  
1180 control (siCtrl) and siRNA targeting the endogenous 3' untranslated region (3'UTR) of KDM6B  
1181 (siKDM6B-3'UTR). 4 days later, cells were stained with crystal violet.

1182 **(K)** Quantification of cell density of each group (n=3) using imageJ. P-value calculated using student t  
1183 test.

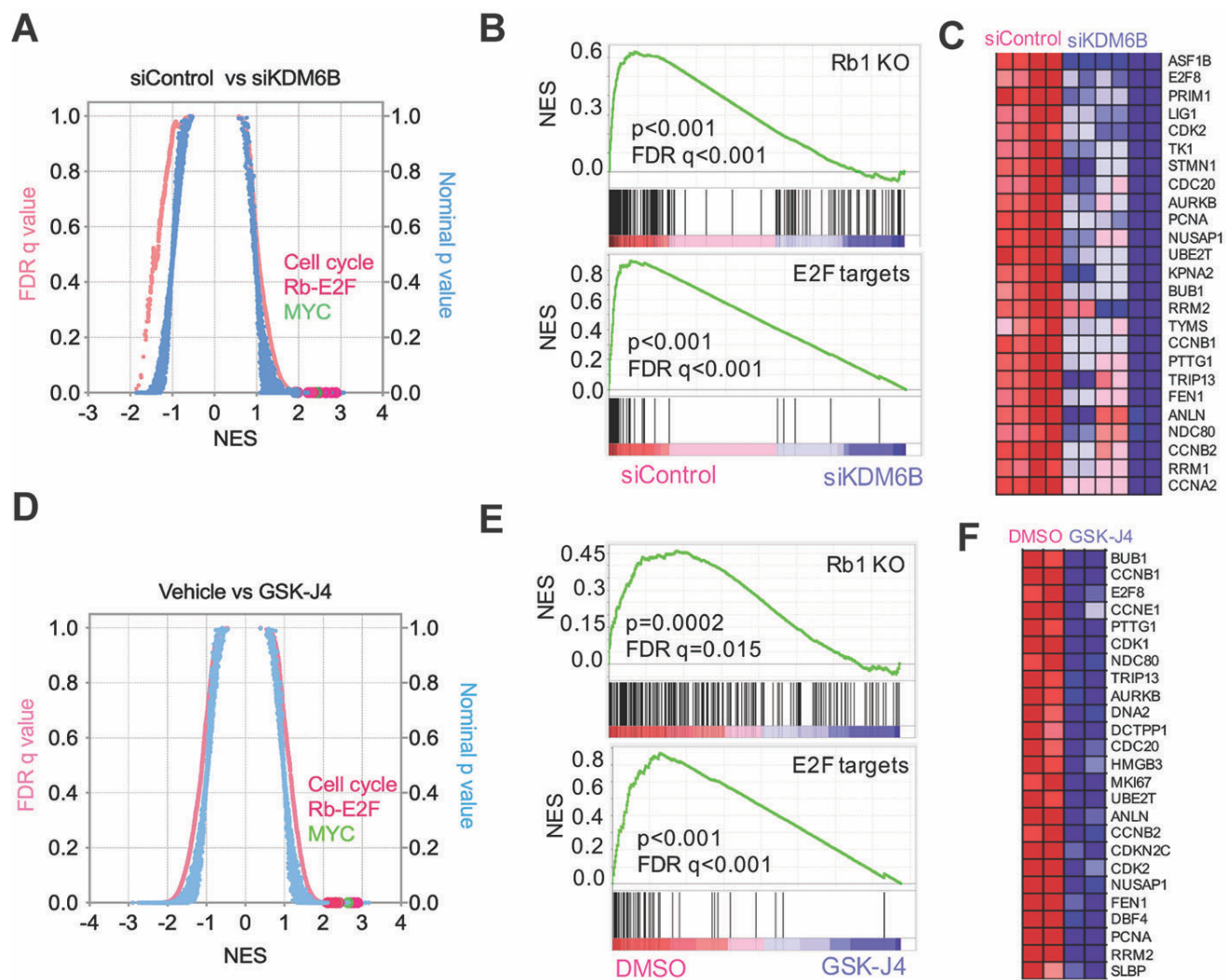
1184 **(L)** BE2C and MSCV-KDM6B overexpressing (KDM6B-OE) BE2C cells were transfected with siRNA  
1185 control (siCtrl) and siRNA siKDM6B-3'UTR. 2 days later, cells were subject to immunoblotting with  
1186 indicated antibodies.

1187

1188

1189





1190 **Figure 2. KDM6B predominantly regulates the pRB-E2F pathway.**

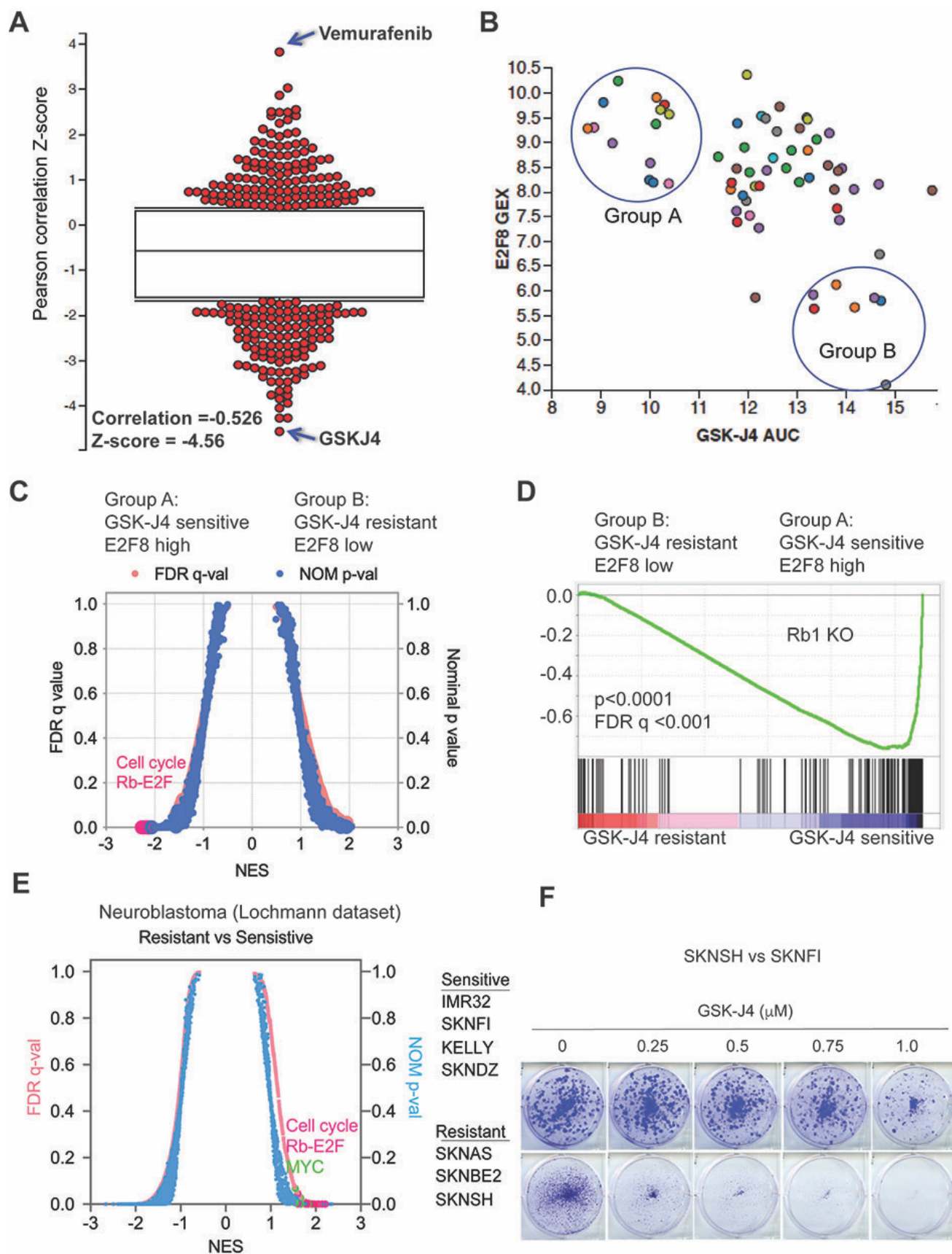
1191 **(A)** Quantitative comparison of all chemical and genetic perturbation gene sets ( $n = 3403$ ) from the  
1192 MSigDB by gene set enrichment analysis (GSEA) for increased (left) and reduced (right) expression of  
1193 global genes caused by KDM6B knockdown. Data are presented as a scatterplot of normalized p  
1194 value/false discovery q value vs normalized enrichment score (NES) for each evaluated gene set. The gene  
1195 sets circled in red color indicate cell cycle, pRB-E2F and MYC pathway gene sets.

1196 **(B)** Two examples of GSEA show that genes downregulated by depletion of KDM6B are enriched with  
1197 Rb1 knockout and E2F targets.

1198 **(C)** Heatmap shows the gene list from the E2F targets (B).

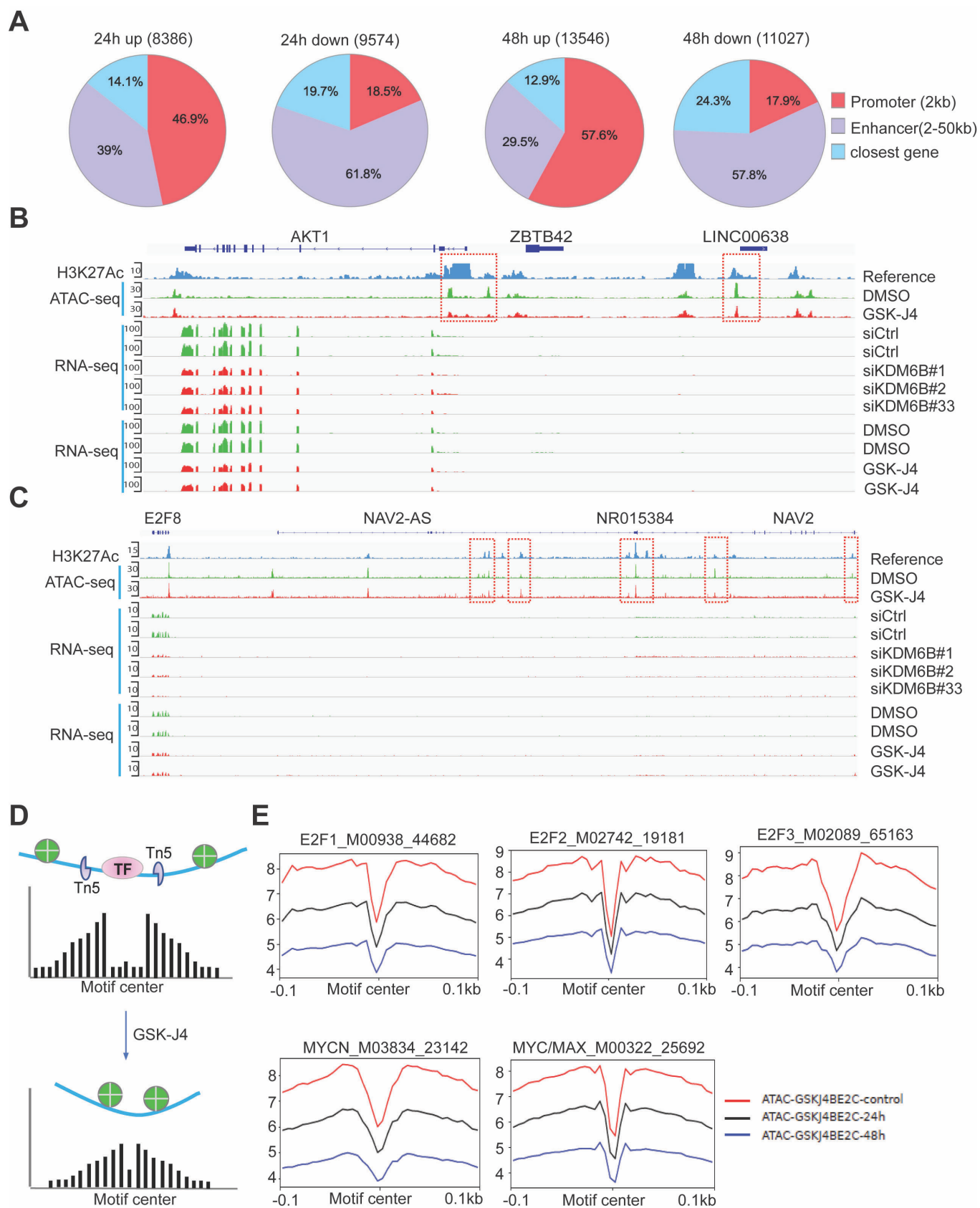
1199 **(D-F)** Similar analysis for GSK-J4 treatment as shown in (A-C).

1200



1201 **Figure 3. Chemogenetic data show E2F gene signature is correlated with sensitivity of GSK-J4.**  
1202 **(A)** The Pearson correlation Z-score for each tested compound with E2F8 expression, which was extracted  
1203 from The Cancer Therapeutics Response Portal (CTRP). The correlation of GSK-J4 and E2F8 ranked on  
1204 the top with  $R=-0.626$ ,  $Z\text{-score}=-4.56$ .  
1205 **(B)** The plot of E2F8 expression and GSK-J4 sensitivity for each tested cell line. The y-axis represents  
1206 the transcript expression levels of E2F8 in each cell line. The x-axis represents the drug response metrics  
1207 (area under curve, AUC) to GSK-J4. The lower the AUC, the more sensitive to GSK-J4. The circled group  
1208 A and B populations are arbitrarily chosen as GSK-J4 sensitive vs resistant.  
1209 **(C)** Quantitative comparison of all chemical and genetic perturbation gene sets ( $n = 3403$ ) from the  
1210 MSigDB by gene set enrichment analysis (GSEA) for GSK-J4 sensitive (group A) and resistant (group  
1211 B). Data are presented as a scatterplot of normalized p value/false discovery q value vs normalized  
1212 enrichment score (NES) for each evaluated gene set. The red dots highlight cell cycle and Rb-E2F pathway  
1213 gene sets.  
1214 **(D)** GSEA show that genes highly expressed in GSK-J4 sensitive (group A) cells are enriched with Rb1  
1215 knockout.  
1216 **(E)** Quantitative comparison of all chemical and genetic perturbation gene sets ( $n = 3403$ ) from the  
1217 MSigDB by gene set enrichment analysis (GSEA) for GSK-J4 sensitive and resistant neuroblastoma cells,  
1218 as shown in the right panel of cell lines. Data are presented as a scatterplot of normalized p value/false  
1219 discovery q value vs normalized enrichment score (NES) for each evaluated gene set. The red and green  
1220 dots highlight cell cycle and Rb-E2F pathway gene sets and MYC gene sets, respectively.  
1221 **(F)** Crystal violet staining of colonies after SK-N-SH and SK-N-FI neuroblastoma cell lines were treated  
1222 with different concentrations of GSK-J4 for 7 days.

1223  
1224  
1225  
1226  
1227  
1228  
1229  
1230  
1231  
1232





1233 **Figure 4. KDM6B inhibition represses chromatin accessibility of E2F genes.**

1234 **(A)** ATAC-seq was performed after BE2C cells were treated with 2.5 $\mu$ M of GSK-J4 for 48 hours.  
1235 Summary of peak calling number of ATAC-seq ( $p < 0.05$ , log<sub>2</sub> fold change  $\geq 0.5$ ) including the  
1236 upregulated and downregulated nucleosome free regions, and the annotated locations of the peaks at  
1237 defined promoter and enhancer regions.

1238 **(B)** Snapshot of *AKT1* locus using Integrative Genomic Viewer (IGV) for ATAC-seq, H3K27Ac ChIP-  
1239 seq, and RNA-seq. The ATAC-seq analysis shows the downregulation of two peaks at the 5' promoter  
1240 region of *AKT1* and one peak at the non-coding RNA *LINC00638*. The RNA-seq results showed that the  
1241 AKT1 transcript was downregulated by 48h of GSK-J4 treatment and KDM6B knockdown. H3K27Ac in  
1242 BE2C cells was referenced to GSM2113518<sup>109</sup>.

1243 **(C)** Snapshot of *E2F8* locus using Integrative Genomic Viewer (IGV) for ATAC-seq, H3K27Ac ChIP-  
1244 seq, and RNA-seq. The ATAC-seq shows the downregulation of three peaks at the enhancer region of  
1245 *E2F8*, next to the *NAV2* gene locus. The RNA-seq results showed that *E2F8* transcript was downregulated  
1246 by KDM6B inhibition while the adjacent *NAV2* expression is barely detectable.

1247 **(D)** Cartoon indicates the rationale of footprinting analysis. The DNA motifs bound by transcription  
1248 factors such as E2F1 protect the cut from transposase Tn5, while the adjacent open chromatin gives rise  
1249 to a high signal of nucleosome free region after ATAC-seq analysis. After GSK-J4 treatment, the open  
1250 chromatin was repressed and consequently reducing the reads of free DNA.

1251 **(E)** Footprinting plot shows the reduction of open chromatin at predicted binding motifs of E2Fs and  
1252 MYC after BE2C cells were treated with GSK-J4 for 24 h and 48h.

1253

1254

1255

1256

1257

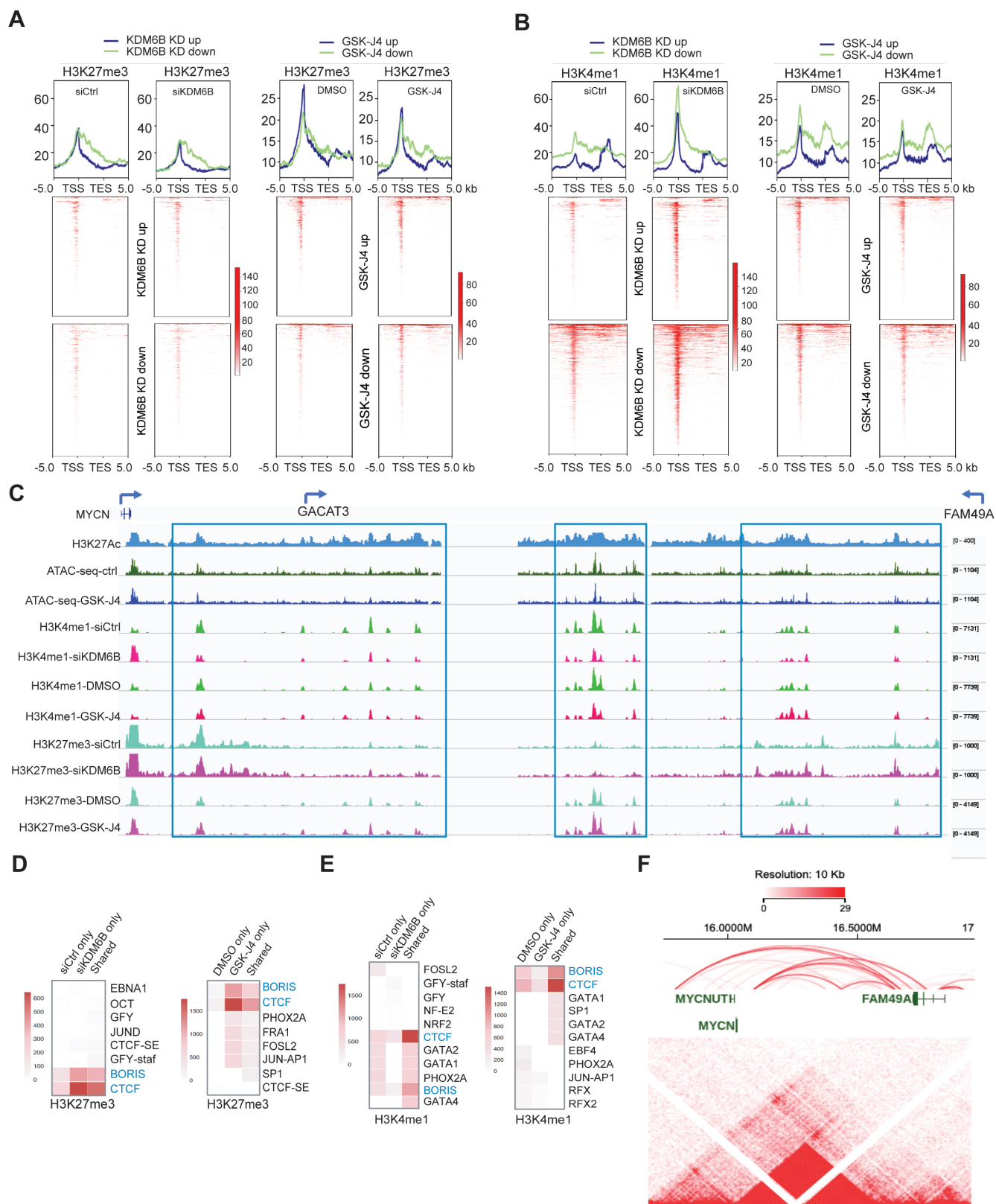
1258

1259

1260

1261

1262



1263 **Figure 5. KDM6B inhibition induces an increase of H3K27me3 but a decrease of the enhancer mark**  
1264 **H3K4me1 at CTCF and BORIS binding sites**

1265 **(A, B)** Heatmap indicating the CUT&Tag signal intensity of H3K27me3 (A) and H3K4me1(B) around  
1266 differentially expressed genes (from TSS-5kb to TES+5kb). CUT&Tag experiments were done with two  
1267 biological replicates in KDM6B knockdown and GSK-J4 treatment respectively. Differentially  
1268 expressed genes were identified by cutoffs ( $\log_2FC > 0.5$ ) from RNA-seq. TSS= transcription start site,  
1269 TES=transcription end site

1270 **(C)** The signals of H3K27me3 and H3K4me1 (CUT&Tag), H3K27Ac (ChIP-seq)<sup>109</sup>, and ATAC-seq  
1271 between the genomic locus of *MYCN*, *GACAT3*, and *FAM149A*, snapshot using IGV program.

1272 **(D, E)** Motif analysis of H3K27me3 (D) and H3K4me1 (E) peaks by using HOMER known motif search.  
1273 Top ten most significant motifs from each sub-group were visualized as a heatmap. The heatmap scale  
1274 indicates  $-\log_{10}(p \text{ value})$ .

1275 **(F)** The Hi-C data of BE2C neuroblastoma cells (data extracted from the St Jude Cloud) showing that  
1276 *MYCN* and its adjacent *FAM149A* locus reside in the same topologically associated domain (TAD). The  
1277 Arc indicates the chromatin interactions, which were generated from Jurkat ChIA-PET SMC1 (Mango)  
1278 (<https://proteinpaint.stjude.org/>).

1279

1280

1281

1282

1283

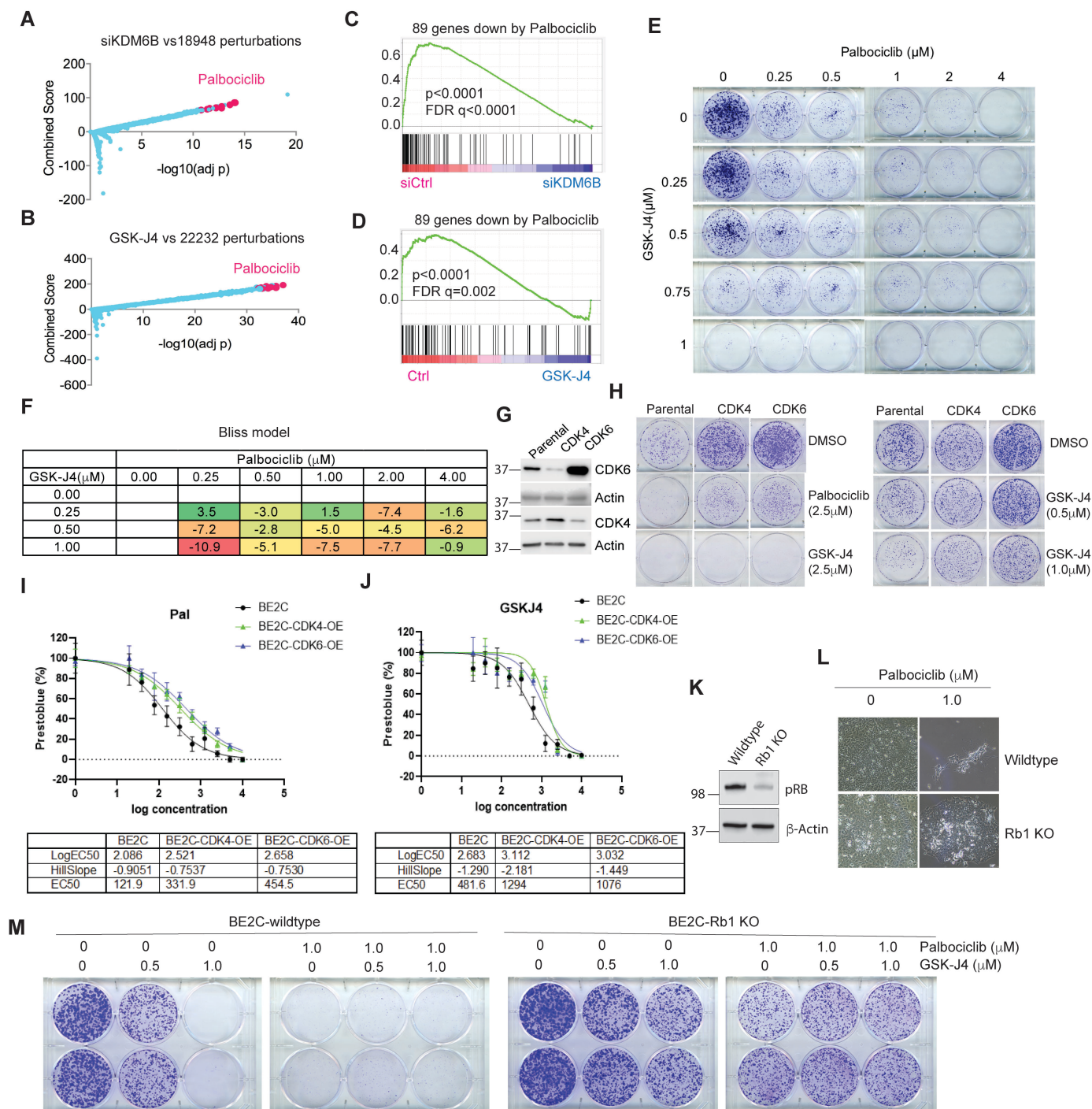
1284

1285

1286

1287

1288



1289 **Figure 6. GSK-J4 induces a transcriptome that mimics CDK4/6 inhibition, and vice versa**

1290 (A) Genes downregulated by KDM6B knockdown were compared with gene profiles induced with  
1291 chemical compounds from Library of Integrated Network-Based Cellular Signatures (LINCS). The top  
1292 chemical signature hits, which are basically overrepresented by palbociclib, are highlighted in pink dots.

1293 (B) Same analysis performed as in (A) for GSK-J4 treatment.

1294 (C) The 89-gene signature derived from palbociclib treatment of 4 neuroblastoma cell lines was included  
1295 in gene sets for GSEA analysis of KDM6B knockdown.

1296 (D) The 89-gene signature derived from palbociclib treatment was included in gene sets for GSEA analysis  
1297 of GSK-J4.

1298 (E) BE2C cells were seeded with low numbers in 6-well plate and treated with different concentrations of  
1299 GSK-J4 or/and palbociclib for 10 days. The cell colonies were stained with crystal violet.

1300 (F) Bliss index for the combination of GSK-J4 and palbociclib. Positive scores indicate synergy, negative  
1301 scores indicate antagonism.

1302 (G) Western blot to assess the expression of CDK4 and CDK6 that were transduced into BE2C cells.

1303 (H) The BE2C parental and CDK4/6 overexpressing cells were seeded with low numbers in 6-well plate  
1304 and treated with different concentrations of GSK-J4 or palbociclib for 8 days. The cell colonies were  
1305 stained with crystal violet.

1306 (I, J) BE2C and CDK4 or CDK6 overexpressing BE2C cells (BE2C-CDK4-OE, BE2C-CDK6-OE) were  
1307 treated with different concentrations of palbociclib (I) or GSK-J4 (J). EC50 was calculated using  
1308 Prestoblue assay.

1309 (K) Western blot to assess the expression of pRB after inducible knockout in BE2C cells.

1310 (L) Photos taken under microscope (10x) show Rb1 knockout leads to resistance to palbociclib.

1311 (M) The BE2C wildtype and Rb1 knockout cells were seeded with low numbers in 6-well plate and treated  
1312 with different concentrations of GSK-J4 or/and palbociclib for 8 days. The cell colonies were stained with  
1313 crystal violet.

1314

1315

1316

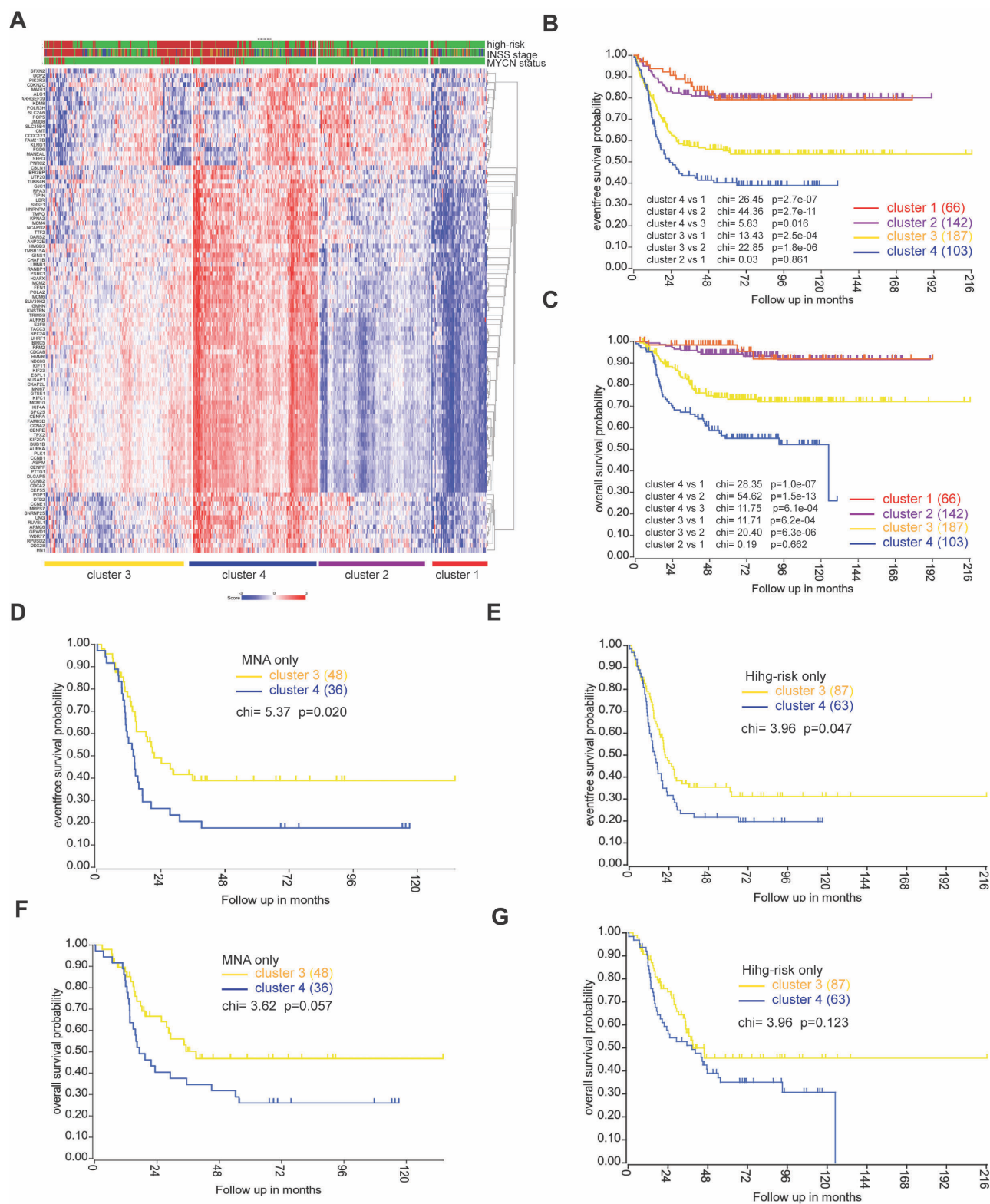
1317

1318

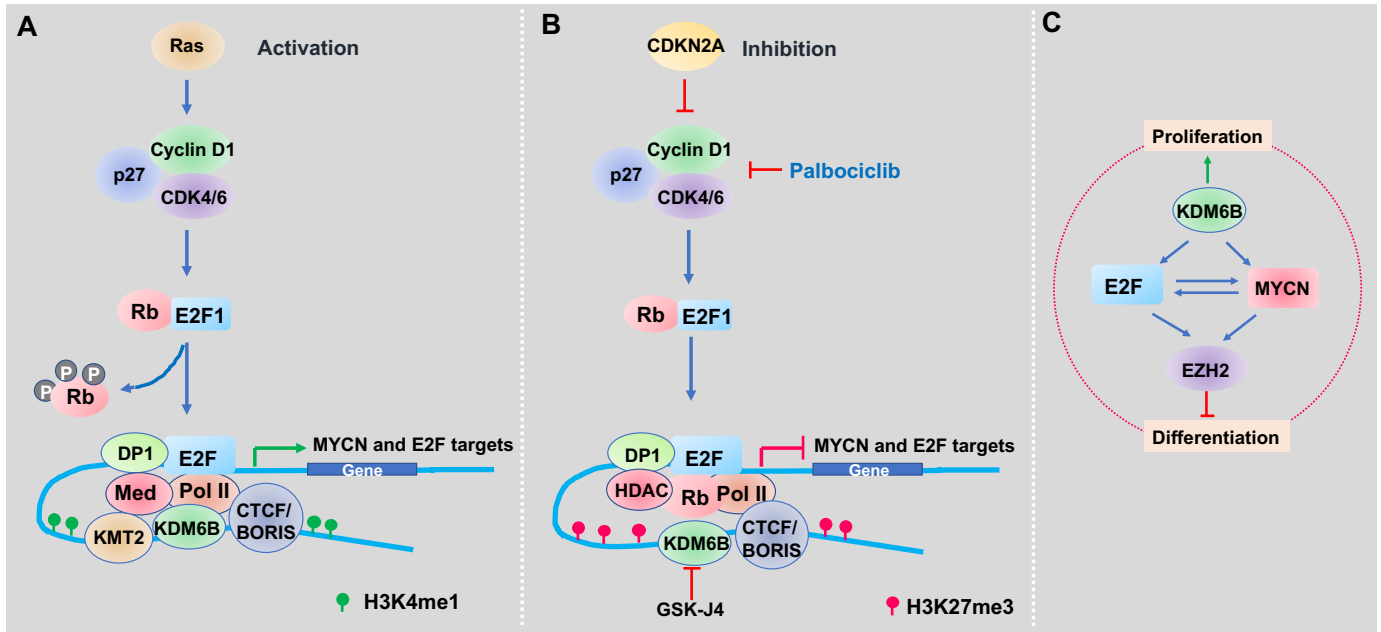
1319

1320





1321 **Figure 7. A gene signature targeted by KDM6B inhibition is associated with poor outcome**  
1322 (A) 149-gene signature was uploaded into R2 genomics analysis program ([https://hgserver1.amc.nl/cgi-](https://hgserver1.amc.nl/cgi-bin/r2/main.cgi)  
1323 [bin/r2/main.cgi](https://hgserver1.amc.nl/cgi-bin/r2/main.cgi)) to find the differentially expressed genes in high-risk neuroblastoma in a cohort dataset  
1324 (GSE49710) that has 498 neuroblastoma cases, followed by k-means cluster analysis. Risk (Red =high  
1325 risk; green =low risk); MYCN (red = Amplification; green = non-Amplification); Stage (red = stage 4;  
1326 blue= stage 4S; brown =stage 3; dark green = stage 2, green= stage 1).  
1327 (B-C) Kaplan-Meier curve using Log-Rank method shows the event-free survival and overall survival of  
1328 4 clusters that have differential expression levels of GSK-J4 signature.  
1329 (D, F) Kaplan-Meier curve using Log-Rank method shows the event-free survival and overall survival of  
1330 clusters 3 and 4 with MNA.  
1331 (E, G) Kaplan-Meier curve using Log-Rank method shows the event-free survival and overall survival of  
1332 clusters 3 and 4 with high-risk disease.  
1333  
1334  
1335  
1336  
1337  
1338  
1339  
1340  
1341  
1342  
1343  
1344  
1345  
1346



1347

1348 **Figure 8. Working model of KDM6B inhibition in neuroblastoma.**

1349 (A) Upon stimulation by mitogens, KDM6B is recruited to chromatin to maintain the low levels of  
 1350 H3K27me3 at the distal regulatory enhancer regions marked by H3K4me1 overlapping with the  
 1351 CTCF/BORIS binding sites, which loops and physically interacts with E2F that binds at the promoter of  
 1352 target genes, together with associated transcriptional machinery including RNA polymerase II and  
 1353 mediators, driving the MYCN and E2F transcriptome.

1354 (B) When inhibited by CDK4/6 inhibitor, the inhibitory pRB complexes with HDAC to suppress gene  
 1355 transcription. When KDM6B is inhibited by GSK-J4, the H3K27me3 will accumulate at the distal regions  
 1356 to displace the H3K4me1 modifier KMT2 and evicts the transcription activators of promoter-enhancer,  
 1357 leading to the downregulation of MYCN and E2F transcriptome (Figure 7B).

1358 (C) A network composed by MYCN, E2F, EZH2 and KDM6B regulates the cell proliferation and  
 1359 differentiation of neuroblastoma.

1360

1361

1362

1363

1364

1365

1366

1367

**Table 1. Transcription factor binding motif enrichment for KDM6B target genes (top15)**

	<b>Gene Sets</b>	<b>NES</b>	<b>NOM p-val</b>	<b>FDR q-val</b>
1	KRCTCNNNNMANAGC_UNKNOWN	2.76	0	0
2	SGCGSSAAA_E2F1DP2_01	2.17	0	0
3	TTTNNANAGCYR_UNKNOWN	2.14	0	0
4	E2F4DP1_01	2.1	0	0
5	E2F_03	2.06	0	0
6	E2F1_Q6	2.03	0	0
7	E2F_02	2.03	0	0
8	E2F_Q6	2.02	0	0
9	E2F_Q3	2.01	0	0
10	E2F4DP2_01	2	0	0
11	E2F1DP2_01	2	0	0
12	E2F1DP1_01	1.99	0	0
13	E2F_Q4	1.99	0	0
14	E2F_Q6_01	1.92	0	0
15	E2F1_Q6_01	1.9	0	0

**Table 2. Transcription factor binding motif enrichment for GSK-J4 target genes (top 15)**

	<b>Gene sets</b>	<b>NES</b>	<b>NOM p-val</b>	<b>FDR q-val</b>
1	KRCTCNNNNMANAGC_UNKNOWN	2.43	0	0
2	SGCGSSAAA_E2F1DP2_01	1.48	0.003	0.253
3	E2F_01	1.42	0.037	0.31
4	E2F_Q3	1.39	0.012	0.325
5	TTTNNANAGCYR_UNKNOWN	1.39	0.023	0.262
6	E2F_Q6	1.36	0.012	0.274
7	E2F1_Q3	1.33	0.015	0.308
8	E2F4DP1_01	1.32	0.018	0.301
9	E2F1_Q6	1.32	0.02	0.269
10	E2F_Q4	1.31	0.013	0.273
11	RGTTAMWNATT_HNF1_01	1.31	0.071	0.25
12	E2F1DP2_01	1.29	0.027	0.268
13	E2F_02	1.28	0.028	0.266
14	E2F1_Q6_01	1.28	0.042	0.255
15	E2F1DP1_01	1.28	0.037	0.246

**Table 3. Transcription factor binding motif enrichment for neuroblastoma cells sensitive to GSK-J4**

	<b>Gene Sets</b>	<b>NES</b>	<b>NOM p-val</b>	<b>FDR q-val</b>
1	E2F_Q6	1.89019	0.00000	0.00000
2	E2F_Q4	1.86916	0.00000	0.00112
3	E2F4DP2_01	1.84061	0.00000	0.00075
4	E2F_Q2	1.83652	0.00000	0.00112
5	E2F1DP1_01	1.83527	0.00000	0.00090
6	E2F1_Q6	1.83142	0.00000	0.00075
7	E2F1DP2_01	1.83124	0.00000	0.00064
8	E2F1_Q3	1.82484	0.00000	0.00056
9	E2F1DP1RB_01	1.80926	0.00000	0.00050
10	E2F4DP1_01	1.80680	0.00000	0.00045
11	E2F_Q3_01	1.80364	0.00000	0.00041
12	E2F_Q3	1.79745	0.00000	0.00064
13	SGCGSSAAA_E2F1DP2_01	1.79145	0.00000	0.00076
14	E2F1_Q4_01	1.77454	0.00000	0.00125
15	E2F_Q4_01	1.77275	0.00000	0.00117
16	E2F_Q6_01	1.71608	0.00000	0.00258
17	E2F1_Q6_01	1.67011	0.00000	0.00468
18	E2F_Q3	1.66943	0.00000	0.00448
19	KRCTCNNNNMANAGC_UNKNOWN	1.63733	0.00184	0.00603
20	NRF1_Q6	1.55445	0.00000	0.01859
21	NRSF_01	1.54447	0.00000	0.01968
22	TMTCGCGANR_UNKNOWN	1.52952	0.00000	0.02146
23	CAGNWMCNNGAC_UNKNOWN	1.52403	0.00000	0.02186
24	ACTAYRNNNCCCR_UNKNOWN	1.51553	0.00000	0.02396
25	MCAATNNNNNGCG_UNKNOWN	1.51439	0.00372	0.02336